WHEN OVERTURNING CIRCULATION BECAME GLOBAL: INSIGHT INTO ITS TIMING FROM NEODYMIUM ISOTOPES OF FOSSIL FISH TEETH/DEBRIS AND FERROMANGANESE OXYHYDROXIDE COATINGS IN THE PACIFIC OCEAN

A Thesis

by

TY D. COBB

Submitted to the Office of Graduate and Professional Studies of
Texas A&M University
in partial fulfillment of the requirements for the degree of

MASTER OF SCIENCE

Chair of Committee,	Deborah J. Thomas
Committee Members,	Kara A. Bogus
	Niall Slowey
Head of Department,	Shari Yvon-Lewis

May 2017

Major Subject: Oceanography

ABSTRACT

Reconstructions of overturning circulation from IODP Sites covering 40-65 Ma indicate a fundamentally different overturning mode (referred to herein as the Paleogene mode) compared to the modern. Significantly different global climate and plate tectonic boundary conditions during this time interval likely contributed to the different mode of overturning circulation in which each major basin was characterized by distinct and restricted overturning circulations. The modern mode more closely resembles one large continuous Global Overturning Circulation. Here, new Nd isotope data from IODP Site U1438 spanning 27 Ma to the present are used to investigate the timing of the transition from the Paleogene mode to the modern mode. Site U1438 is situated at 4720 m water depth and is ideal to record relative contributions of deep-water masses from the North Pacific and those sourced from the Pacific sector of the Southern Ocean (e.g., Antarctic Bottom Water). The Nd isotopic record collected at U1438 reflects that the shift from the Paleogene mode to the modern mode occurred by 14 Ma, coinciding with the large shift in climate from a relatively warm world to a gradually cooling world that was established by the end of the MMCO. However, the data suggest that at least some part (e.g., 14.8 Ma) of the water mass composition recorded at Site U1438 may have been overprinted by other contributions of dissolved Nd. Given its proximity to contemporaneous volcanic inputs, it is likely that relatively labile volcaniclastic materials partially dissolving at the seafloor and within pore waters potentially affected

the ε_{Nd} composition. This study highlights the need to thoroughly characterize the potential inputs of dissolved Nd to a given location before incorporating a new Nd isotope record into the reconstruction of global deep-water circulation.

For Mom.

ACKNOWLEDGEMENTS

I would like to thank my committee chair, Dr. Debbie Thomas, who has supported and guided me through so much. Also, thank you to my committee members, Dr. Kara Bogus, and Dr. Niall Slowey, for their guidance and support throughout the course of this research. To Dr. Sev Kender, who was also a key part of this project, thank you for your support and advice.

Thanks also go to my friends and colleagues and the department faculty and staff for making my time at Texas A&M University a great experience. A special thank you goes to Claire McKinley, Jenna Newman, Zach Rolewicz, and Rachel Scudder, for their patience and guidance in the radiogenic clean lab as well as for being extremely supportive. Also, thank you to everyone at the International Ocean Discovery Program, which was fundamental in the success of this project.

Finally, thanks to my Mom and Dad for their encouragement, love, and support. Without you I would not be here today. Lastly, thank you to my closest friends who stood by me through the impossible no matter what, you know who you are, I love you.

NOMENCLATURE

Elements

Ca	Calcium
CO_2	Carbon Dioxide
Fe	Iron
Mg	Magnesium
Mn	Manganese
Nd	Neodymium
Pb	Lead
Re	Rhenium
REE	Rare Earth Element
Sm	Samarium

Chemicals

HCl	Hydrochloric Acid
HF	Hydrofluoric Acid
HNO_3	Nitric Acid
HH	Hydroxylamine Hydrochloride

Units

Da	Dalton (1.66×10^{-27} kg)
Ma	Million Years Ago
mbsf	Meters Below Sea Floor
ppm	Parts Per Million
μm	Microns
μL	Microliter
Sv	Sverdrup

Water Masses

AABW	Antarctic Bottom Water
AAIW	Antarctic Intermediate Water
ACC	Antarctic Circumpolar Current
CDW	Circumpolar Deep Water
IDW	Indian Deep Water
LCDW	Lower Circumpolar Deep Water
NADW	North Atlantic Deep Water
NPDW	North Pacific Deep Water
SPDW	South Pacific Deep Water
PDW	Pacific Deep Water
UCDW	Upper Circumpolar Deep Water

Other

AMOC	Atlantic Meridional Overturning Circulation
CC	Core Catcher
CCD	Carbonate Compensation Depth
CHUR	Chondritic Uniform Reservoir
DSDP	Deep Sea Drilling Project
EAIS	East Antarctic Ice Sheet
GOC	Global Overturning Circulation
IODP	International Ocean Discovery Program
KPR	Kyushu-Palau Ridge
MMCO	Mid-Miocene Climatic Optimum
Milli-Q	Ultrapure Water
MOC	Meridional Overturning Circulation
ODP	Ocean Drilling Program
SST	Sea Surface Temperature
TIMS	Thermal Ionization Mass Spectrometer

CONTRIBUTORS AND FUNDING SOURCES

Contributors

This work was supported by a thesis committee consisting of Professor Debbie Thomas and Professor Niall Slowey of the Department of Oceanography and Dr. Kara Bogus of the International Ocean Discovery Program.

The data analyzed was provided by the International Ocean Discovery Program from Expedition 351.

All work for the thesis was completed by the student, under the advisement of Debbie Thomas of the Department of Oceanography.

Funding Sources

There are no outside funding contributions to acknowledge related to the research and compilation of this document.

TABLE OF CONTENTS

Page

ABSTRACT ii

DEDICATION. iv

ACKNOWLEDGEMENTS v

NOMENCLATURE vi

CONTRIBUTORS AND FUNDING SOURCES viii

TABLE OF CONTENTS ix

LIST OF FIGURES vii

LIST OF TABLES xii

1. INTRODUCTION 1

2. BACKGROUND 4

2.1 Modern Thermohaline Circulation 4
2.2 Marine Geochemical Cycling of Neodymium 6
2.3 Neodymium as a Water Mass Tracer 7
2.4 Paleogene Overturning Circulation Mode 11
2.5 Neogene Climate 14
2.6 Neogene Overturning Circulation and Establishment of the Modern Mode 16

3. SAMPLES AND METHODS 18

3.1 IODP Site U1438 18
3.2 Analytical Methods 20

4. RESULTS 23

5. DISCUSSION 28

5.1 U1438 Nd Signature 28
5.2 Regional Comparison 35
5.3 Site U1438 Global Implications 40

6. CONCLUSION 42

REFERENCES 44

LIST OF FIGURES

Page

Figure 1. Schematic of the modern overturning circulation.....5

Figure 2. Compilation of different simulations and mixing from Thomas et al. [2014]..14

Figure 3. Relevant Pacific Ocean sites in this study 19

Figure 4. Lithology, sedimentation rate and age model based reconstruction of Site U1438 19

Figure 5. Fish teeth/debris, Fe-Mn oxide coatings, and Detrital $\varepsilon_{Nd}(t)$ values for Site U1438 24

Figure 6. Fish teeth ε_{Nd} values compared to Fe-Mn oxide coatings.....25

Figure 7. Site U1438 – 14HCC 33

Figure 8. Compilation of new data and existing data 34

Figure 9. The εNd(t) values of Sites U1438 and 786A from Kender et al. [in review] ...39

LIST OF TABLES

Page

Table 1. Site U1438 Nd isotope data from fossil fish teeth/debris.....26

Table 2. Site U1438 Nd isotope data from Fe-Mn oxyhydroxide coatings 27

Table 3. Site U1438 Nd isotope data from detrital silicates.....27

1. INTRODUCTION

Today, it is unclear how continued warming will affect oceanic convection rates and heat transport. Model simulations predict a decrease in deep-water convection by up to 50% based on the observed ~0.5ºC increase of global average sea surface temperatures over the past 135 years [*Gregory et al.*, 2005; *Park et al.*, 2014]. Changes in the rate of deep-water convection will likely affect global heat transport, a process that strongly influences transient climate change [*Gregory*, 2000]. A growing body of paleoceanographic data indicates that changes in global overturning circulation (GOC) have contributed to climate variations on decadal to multi-million year timescales. Looking at how changes in past global ocean circulation relate to Cenozoic cooling trends is crucial to understanding how continued warming will impact both convection rates and heat transport [*Gregory et al.*, 2005; *Hague et al.*, 2012; *Sluijs et al.*, 2008; *Thomas et al.*, 2014; *Via et al.*, 2006; *Zachos et al.*, 2008; *Zika et al.*, 2015].

During the Cenozoic, there have been different modes of deep-water circulation in the Pacific Ocean. *Thomas et al.* [2014] showed that a bipolar mode of convection existed in the Pacific that was independent of the Atlantic Meridional Overturning Circulation (AMOC). This mode resulted in each basin possessing its own distinct overturning circulation. The Paleogene mode, which occurred during the much warmer early Cenozoic, contained two distinct water masses (North Pacific Deep Water (NPDW) and South Pacific Deep Water (SPDW)) that were independent from the Atlantic, whereas the modern mode consists of one large continuous GOC ending in the Pacific. The exact

timing of the shift between these two modes has yet to be determined; this prompts the question, when did the Paleogene mode cease and give way to modern GOC? This is a crucial question for paleoceanographic studies as it marks the point at which Circumpolar Deep Water (CDW) began to dominate the deepest basins and NPDW disappeared.

Neodymium (Nd) isotopes of fossil fish teeth and debris [*Thomas,* 2004], Fe-Mn oxide coatings [*Abbott et al.*, 2015; *Abbott et al.*, 2016; *Molina-Kescher et al.*, 2014; *Xie et al.*, 2012] and Fe-Mn crusts [*Ling et al.*, 1997; *van de Flierdt et al.*, 2004a] are robust tracers of water mass composition. Nd isotopic data collected from Ocean Drilling Program (ODP) Sites 1209 and 1211 indicate contributions from North Pacific deep-water (e.g., the Paleogene mode) began ~65 Ma, continued for ~20 Myr, and began to decrease by ~45 Ma as the contribution from the North Pacific mixed with waters originating from the South Pacific. The shift from the Paleogene mode to the modern mode is thought to have occurred after ~30 Ma [*Thomas et al.*, 2014], but the timing is not well-constrained.

To answer the question of when deep ocean circulation switched modes, more Nd isotope records from the Pacific Ocean are required that cover the Neogene, particularly within the abyssal Northwest Pacific Ocean. In this study, a new Nd isotope record, derived from fish teeth/debris and authigenic Fe-Mn oxyhydroxides coatings, allows insight into the behavior of Nd at water mass boundaries within abyssal water during this time period (~27-0 Ma), allowing for a more comprehensive constraint on Pacific

circulation. Located in the Northwest Pacific at a current water depth of 4720 m, Site U1438 is ideally situated to capture a record of the deep-water flux within the North Pacific (referred to here as NPDW; e.g., *Hague et al.* [2012] and *Thomas et al.* [2014]) and the record of deep-water sourced from the Pacific sector of the Southern Ocean SPDW from *Thomas et al.* [2014].

2. BACKGROUND

2.1 Modern Thermohaline Circulation

In the modern ocean, the GOC is characterized by the wind-driven sinking of cold, saline waters at high latitudes, which contributes a substantial amount to poleward heat transport [*Talley*, 2013]. The GOC collectively refers to the surface ventilated North Atlantic Deep Water (NADW), the diffusely formed Indian Deep Water (IDW), Antarctic Bottom Water (AABW), and Pacific Deep Water (PDW) (Fig. 1) [*Talley*, 2013]. From the North Atlantic, GOC moves southward, upwelling in the Southern Ocean to form CDW. In the Weddell Sea and western Ross Sea, south of the Antarctic Circumpolar Current (ACC), NADW upwells where new water of the same density is produced and forms the Lower CDW (LCDW) – characterized by a salinity of >34.6 ppm and a density (σ_4) >45.86 kg m^{-3}. Within the ACC and north of NADW, the less dense IDW and PDW upwell to create the Upper CDW (UCDW) which is identified by low oxygen, average salinity ~34.6 ppm, and an average density (σ_θ) of 27.65 kg m^{-3} [*Horikawa et al.*, 2011; *Talley*, 2013]. Along the shelf regions of Antarctica (Weddell Sea, the Ross Sea, and the Adelie Land Prydz Bay), sea ice formation and the resulting brine rejection produces dense water that sinks and forms AABW. Some of the highest density AABW is confined by Southern Ocean topographic sills and ridges but a vast majority, ~32 Sv (1 Sverdrup = 1×10^6 m^3 s^{-1}), escapes into the Weddell and Ross Seas before moving northward into the bottoms of the Atlantic, Indian, and Pacific oceans. As AABW and CDW travel northward into these three basins, they upwell and mix with IDW, PDW, and NADW near the subtropics and tropics. However, AABW does not

extend north of ~ 60°S in the Pacific sector, as it is effectively blocked by the NE-SW oriented Pacific-Antarctic ridge (60°S, 180°W-140°W) [*Horikawa et al.*, 2011; *Orsi et al.*, 1999]. Even so, the upwelled AABW is the sole source of PDW because there is no deep-water formation within the North Pacific [*Broecker*, 2010; *Talley*, 2013].

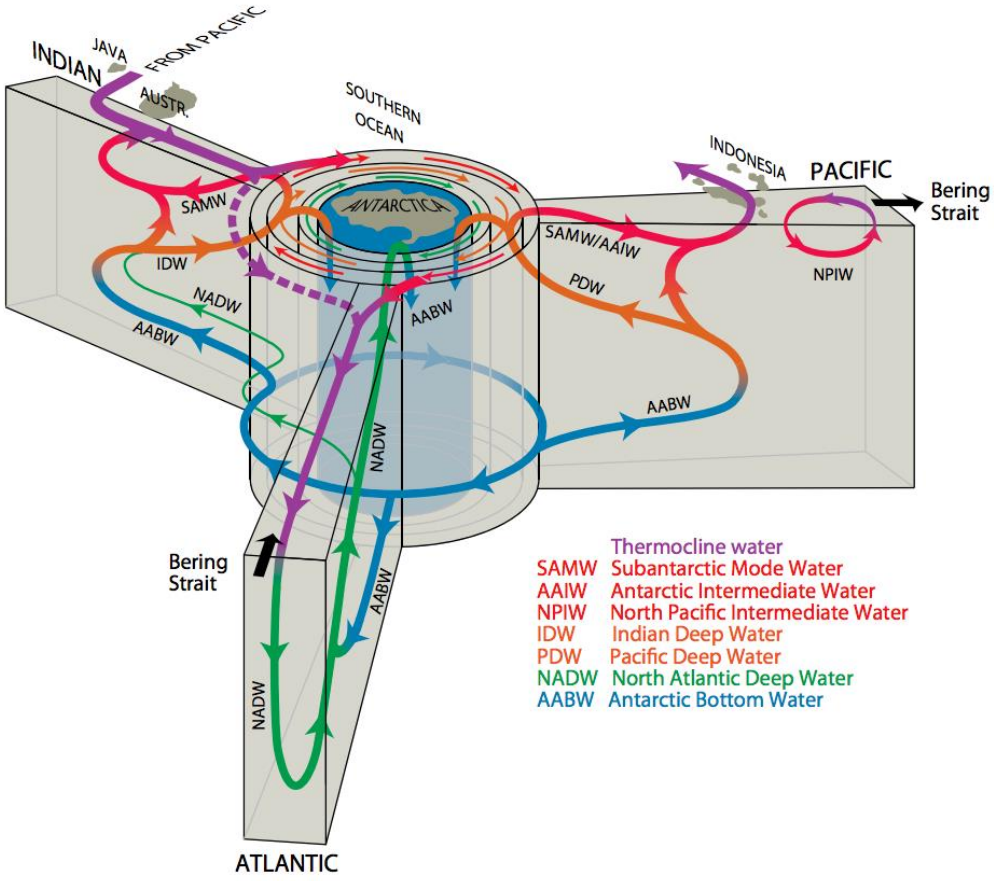

Figure 1. Schematic of the modern overturning circulation. This schematic is from the perspective of the Southern Ocean from *Talley* [2013].

2.2 Marine Geochemical Cycling of Neodymium

^{143}Nd is the daughter isotope of ^{147}Sm which decays via α-decay and has a half-life of 106 Gyr [*Faure and Mensing*, 2005]. These two elements are both incompatible leading to the preferential fractionation into a melt phase over a solid phase. Nd is slightly less compatible than Sm, thus Nd will preferentially migrate from the mantle to the crust during formation, causing crustal rocks to be enriched with Nd [*Goldstein and Hemming*, 2003]. Thus, the Sm/Nd ratio in the residual mantle increases over time, leading to a higher $^{143}Nd/^{144}Nd$ ratio [*Faure and Mensing*, 2005]. However, small variations in the $^{143}Nd/^{144}Nd$ ratio evolve over time, and to simplify the description of the variations, the $^{143}Nd/^{144}Nd$ ratio is interpreted as a deviation from the chondritic uniform reservoir (CHUR) model ($[^{143}Nd/^{144}Nd]_{CHUR} = 0.512638$) in parts per ten thousand:

$$\varepsilon_{Nd} = ([^{143}Nd/^{144}Nd]_0/[^{143}Nd/^{144}Nd]_{CHUR} - 1)\times 10{,}000$$

[*DePaolo and Wasserburg*, 1976; *Faure and Mensing*, 2005; *Frank*, 2002; *Goldstein and Hemming*, 2003; *Goldstein and Jacobsen*, 1987]. The ε_{Nd} values of ancient samples are corrected for in-situ production of ^{143}Nd from the decay of ^{147}Sm post-incorporation into the sample, and these values are interpreted as $\varepsilon_{Nd}(t)$:

$$\varepsilon_{Nd}(t) = ([^{143}Nd/^{144}Nd]_{\text{initial sample}}/[^{143}Nd/^{144}Nd]_{t\ CHUR} - 1)\times 10{,}000$$

where CHUR is the ratio at a given time *t* [*Faure and Mensing*, 2005]. Older continental rocks that are characterized by low concentrations of Sm evolve low $^{143}Nd/^{144}Nd$ concentrations, resulting in highly negative, nonradiogenic ε_{Nd} values, whereas more recently mantle-derived rocks evolve higher Sm and $^{143}Nd/^{144}Nd$ concentrations leading

to more radiogenic ε_{Nd} values [*DePaolo and Wasserburg*, 1976; *Faure and Mensing*, 2005; *Goldstein and Hemming*, 2003; *Goldstein and Jacobsen*, 1987].

One of the major sources of dissolved Nd to the oceans is from fluvial inputs of weathered subaerially exposed rocks and soils [*Elderfield and Greaves*, 1982; *Elderfield et al.*, 1988; *Goldstein and Jacobsen*, 1987; *Halliday et al.*, 1992; *Jones et al.*, 1994]. It has been shown that at least 90% of the Nd concentration that is delivered to the oceans is transported via colloids (particle size between 0.2 µm and 3000 Da) [*Ingri et al.*, 2000]. The distinct distribution of Nd isotopic values is determined by the source rock lithology and age in each ocean basin where an individual water mass forms [*Jones et al.*, 1994]. Nd can also be released from resuspended sediments [*Goldstein and O'Nions*, 1981] or the diagenesis of particles sourced from terrigenous input (riverine and eolian) [*Elderfield and Sholkovitz*, 1987]. Regional contributions of marine sediments are also a large contributor of Nd to the oceans, in the Pacific these benthic sources are believed to control much of the deep-water Nd distribution. The Nd signature is controlled by a combination of circulation pathways and the amount of time an individual water mass is exposed to sedimentary fluxes [*Abbott et al.*, 2015]. *Arsouze et al.* [2009] concluded through different simulations that ~95% of the total dissolved Nd is sourced through sediment dissolution.

2.3 Neodymium as a Water Mass Tracer

The Nd isotopic composition of seawater is one of the most robust tracers of bottom water masses – acquiring and mostly conserving their isotopic signature from the source

region in which they sink [*Elderfield and Greaves*, 1982; *Elderfield et al.*, 1988; *Goldstein and Jacobsen*, 1987]. Nd has a short oceanic residence time (~200–1000 yrs; e.g., *Tachikawa et al.* [1999]) compared to that of oceanic mixing rates (~1500 yrs) creating inter- and intra-basin variations in deep-water composition [*Broecker et al.*, 1960]. Each distinct water mass obtains its unique isotopic fingerprint of Nd from the continental input of the region in which it originates [*Elderfield and Greaves*, 1982; *Elderfield et al.*, 1988; *Goldstein and Hemming*, 2003; *Goldstein and Jacobsen*, 1987]. Modern Pacific Ocean waters have the most radiogenic ε_{Nd} values of ~0 to -4 [*Piepgras and Jacobsen*, 1988] representing an average fluvial input of -2.9 to -3.7 derived from the young arc terrains of Japan, the Philippines, and East Australia [*Goldstein and Jacobsen*, 1987]. Modern Southern Ocean waters (Antarctic Bottom Intermediate Water (AAIW) and AABW) have a less radiogenic signature of ~-8 to -9, which reflects the mixing between a nonradiogenic NADW (ε_{Nd} = ~-12 to -13) and Pacific waters as they flow eastward through the Drake Passage as part of the CDW [*Piepgras and Jacobsen*, 1988; *Talley*, 2013].

There are exceptions to the Nd conservative properties within a water mass that recently have been under discussion [*Abbott et al.*, 2015; *Abbott et al.*, 2016; *Amakawa et al.*, 2009; *Lacan and Jeandel*, 2004; *Lacan and Jeandel*, 2005; *Lacan et al.*, 2012; *Martin and Haley*, 2000; *Molina-Kescher et al.*, 2014; *van de Flierdt et al.*, 2004b]. A discussion that has led to the defining of Nd behavior in proximity to continental margins where it has been shown to be released or absorbed in a process referred to as

boundary exchange [*Lacan and Jeandel*, 2005]. This process can significantly influence the seawater Nd isotopic composition and can represents up to 64% of the total dissolved Nd [*Arsouze et al.*, 2009]. This non-conservative behavior presents a complication when using Nd as a water mass tracer, but there is confidence for most studies (e.g., *Lambelet et al.* [2016]) that Nd can indeed be used as a proxy for water masses [*Frank*, 2002].

In addition to the regional differences between oceanic basins (i.e., Pacific vs. Southern oceans), records of Nd isotopic composition indicate differences between the North Pacific and the South Pacific waters. Despite well-defined intermediate, deep, and bottom waters, Nd depth profiles show that the North Pacific is far less stratified [*Talley*, 1993] than the South Pacific, where surface waters are highly radiogenic ($\varepsilon_{Nd} = 0$) and underlain by less radiogenic waters ($\varepsilon_{Nd} = -8$ at 4500 m water depth) due to a greater influence from AABW [*Amakawa et al.*, 2009; *Carter et al.*, 2012; *Schmitz*, 1996; *Thomas et al.*, 2014]. In the North Pacific, slow deep-water renewal stabilizes the vertical movement of Nd from the surface waters to the deep waters. As Nd descends from the surface waters it interacts with the CDW signal [*Piepgras and Wasserburg*, 1982], resulting in well-mixed relatively radiogenic bottom waters even with the absence of convection [*Broecker*, 2010; *Talley*, 2003; 2013].

Fossil fish teeth and debris (bones and scales; e.g., *Staudigel et al.* [1985]) record the Nd isotopic signature of the water mass at the sea floor post-deposition and therefore create a stratigraphic record of Nd at a given site [*Thomas et al.*, 2014]. Fossil fish teeth are

advantageous for paleoceanographic investigation due to their high concentrations of Nd (100 to >1000 ppm) and their abundance within the world's oceans. The hydroxyfluorapatite of fossil fish teeth is 3 to 6 orders of magnitude larger in Nd concentration than the hydroxyapatite of living fish teeth and therefore supports incorporation of Nd into teeth post-deposition [*Martin and Haley*, 2000]. Authigenic Fe-Mn oxide coatings (e.g., coatings on sediment grains) incorporating seawater Nd reflect the isotopic composition of the ambient seawater in which they formed [*Goldstein and Hemming*, 2003]. This feature makes Fe-Mn oxide coatings a valuable proxy of Nd as they are readily available and allow high spatial and temporal coverage.

However, special consideration must be taken in terms of which acid-reductive leaching technique is used to ensure the reagent attacks the correct fraction within the sample [*Molina-Kescher et al.*, 2014; *Xie et al.*, 2012]. Here, acetic acid was used to separate the metals bound to the carbonate fraction and then hydroxylamine hydrochloride (HH) was used to leach off the Fe- and Mn-oxide fraction. This study utilizes the Nd isotopic composition of fossil fish teeth and debris, Fe-Mn oxide coatings of the sediments, and detrital silicates (e.g., regional weathering inputs) to reconstruct the composition of the deep-water masses from the late Paleogene (~30 Ma) to the present.

Studies of core-top (modern) fish teeth Nd isotopes from the North Pacific show that values do not appear to accurately record bottom water values in the western Pacific [*Horikawa et al.*, 2011]. *Horikawa et al.* [2011] finds that while in both the Central

Pacific and Eastern Equatorial Pacific the core-top fish teeth records support the assumption that Nd is a reliable seawater proxy, this is not necessarily the case in the Northwestern Pacific. The data they present produces significant discrepancies to nearby bottom water, inferring that the fish teeth/debris is out of equilibrium with the bottom seawater. There are several possibilities that could cause such an effect, such as small offsets in location resulting in large variations in the ε_{Nd} regional values [*Amakawa et al.*, 2004] and unfiltered seawater samples that could have contributed particulates capable of decreasing the measured values as much as ~1 ε_{Nd}. They infer that even with the significant discrepancies the fossil fish teeth are in fact in equilibrium with the regional Pacific bottom water Nd isotopes [*Horikawa et al.*, 2011].

The geographic location of Site U1438 and the depth at which it resides (4.7 km mbsf) make it ideal for recording any changes in deep-water within the Northwestern Pacific. U1438 has gradually rotated northward from a position of about 5^{o}N in the Eocene [*Whittaker et al., 2007*], such that it may have moved from approximately 15^{o}N to its current position of 27^{o}N over the past ~25 Ma. This gives the Site the potential to record the northern segment of Pacific deep-water during the Paleogene mode and any changes that occurred to deep-water (e.g., LCDW) during the remainder of the Neogene.

2.4 Paleogene Overturning Circulation Mode

The climate of the Early Paleogene (~65 to 45 Ma) is the most recent major greenhouse interval in Earth history, characterized by warmer mean global temperatures [*Hollis et al.*, 2009; *Zachos et al.*, 2008] and high atmospheric CO_2 levels (>1500 ppm) [*Gregory*

et al., 2005; *Zachos et al.*, 2008]. Sea surface temperatures (SSTs) of the Arctic (15-18°C; e.g., *Sluijs et al.* [2006]) and tropics (28-32°C) in the Early Paleogene indicate that the equator-to-pole temperature gradient during this time was around half the modern gradient [*Pearson et al.*, 2001]. Similarly, previous reconstructions show that gradients in deep-ocean temperature (8-15°C) and the equator-to-pole thermal gradient were weaker in the Paleogene than in the modern ocean [*Hollis et al.*, 2009; *Sluijs et al.*, 2008; *Zachos et al.*, 2008; *Zachos et al.*, 2001]. Previous reconstructions from DSDP, ODP, and IODP Sites using Nd records show a vastly different mode of circulation during the late Cretaceous and early Paleogene (~70 to 43 Ma) compared to the modern [*Hague et al.*, 2012; *Hollis et al.*, 2009; *Sluijs et al.*, 2008; *Thomas*, 2004; 2005; *Thomas et al.*, 2014; *Via et al.*, 2006], and that the shift from the Paleogene mode to the modern GOC coincided with the long term shift from a greenhouse to icehouse world, beginning with the onset of Oligocene glaciation (Oi-1, ~33.4 Ma) [*Zachos et al.*, 2008].

Within the ancient (>30 Ma) Pacific Ocean, Nd isotopes suggest that a north-south geographic gradient existed. There were relatively radiogenic Nd values in the North Pacific (NPDW), nonradiogenic Nd values in the South Pacific (South Pacific Deep-Water (SPDW)), and an intermediate range throughout the mid-latitudes towards the end of the Mesozoic and much of the early Cenozoic (~70 to 30 Ma) [*Thomas et al.*, 2014]. This suggests that during this time distinct individual deep-water masses convected in each of the separate basins. Comparatively, in the modern mode of circulation, Pacific deep-water is only formed through diffusivity [*Talley*, 2013].

In the early Cenozoic, the North Atlantic basin was much more restricted than present. Deep-water formation in the North Atlantic was confined to a latitudinal band (50-60°N) during the early Paleogene, compared to 65-75°N in the Holocene [*Saunders et al.*, 2013]. The opening of the Norwegian and Greenland seas did not occur until the late Paleocene/early Eocene (~55 Ma). As a result, there was no deep-water formation in that area during the Paleocene. Additionally, the Tethyan and Panamanian seaways connected the Atlantic Ocean to the Pacific Ocean, while the Tasmanian Gateway and Drake Passage were not yet open to deep ocean currents [*Frakes and Kemp*, 1972; *Keigwin*, 1982; *Ling et al.*, 1997; *Scher and Martin*, 2006]. The data demonstrate that Southern Ocean waters influenced most of the Pacific, except for the most northern locations, by ~40 Ma. As the Tasmanian Gateway and Drake Passage (~34 Ma) began to open, the connection between the Atlantic and Pacific increased [*Scher and Martin*, 2006]. Even so, evidence supports the assertion that Pacific MOC maintained an individual circulation from the Atlantic MOC at least until that time [*Abbott et al.*, 2016; *Thomas et al.*, 2014]. Simulations show that optimal conditions for such a scenario are explained by intense vertical mixing, predominantly in the abyssal ocean (Fig. 2D, E) [*Thomas et al.*, 2014]. Tidal mixing, internal wave interaction, and heat flow caused by a young and shallow seafloor during the late Cretaceous and early Paleogene help achieve such abyssal mixing [*Thomas et al.*, 2014].

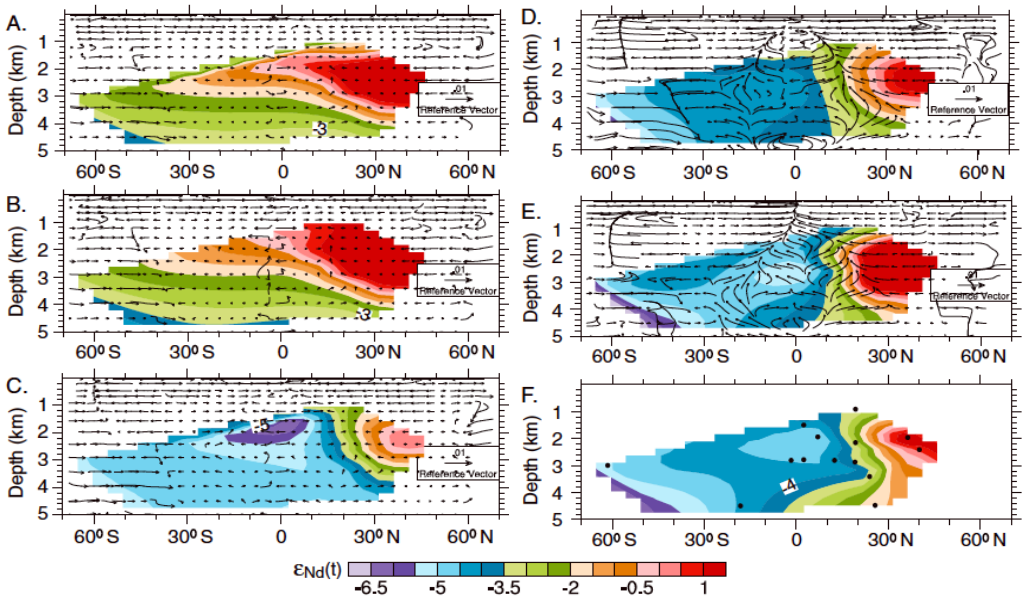

Figure 2. Compilation of different simulations and mixing from *Thomas et al.* [2014]. (a) Warm simulation with normal mixing. (b) Very warm simulation with normal mixing. (c) Very warm simulation with moderate mixing. (d) Very warm simulation with strong abyssal mixing. (e) Very warm simulation with strong mixing. (f) Natural neighbor interpolation of the Pacific $\varepsilon_{Nd}(t)$ records. This data is plotted at its 60 Ma paleopositions and paleodepths (dots represent core paleopositions). In Figures 6a -6e, a transect through the paleo-Pacific of model derived-vertical and meridional velocity vectors (m/s) are overlain onto model-predicted $\varepsilon_{Nd}(t)$ values which are of the same geographic sampling as Figure 6f. All vertical velocities are multiplied by $1x10^4$ for clarity.

2.5 Neogene Climate

During the Neogene (~23 to 2.6 Ma), global climate differed from the Paleogene, with global mean temperature gradually decreasing with a few interspersed warm periods [*Lyle et al.*, 2008]. There are several events during this time that had a large effect on climate, such as the Mid-Miocene Climatic Optimum (MMCO, 17-14.7 Ma) [*Holbourn et al.*, 2015; *Shevenell et al.*, 2008], the formation of the East Antarctica Ice Sheet (EAIS, 13.8 Ma; e.g., *Holbourn et al.* [2014]), and the gradual closure of the Indo-

Pacific Seaway (21 Ma; e.g., *Woodruff and Savin* [1989]) [*Romine and Lombari*, 1985]. These events led to the steepening of ocean temperature gradients and strengthening of the equator-to-pole thermal gradient [*Herbert et al.*, 2016; *Pound et al.*, 2012]. In the deep ocean, *Lear et al.* [2015] found that Neogene Pacific deep-water temperatures began cooling from 15.5 to 14.5 Ma based on benthic foraminiferal $\delta^{18}O$ data. In the late Miocene (9-7 Ma), there are inferential changes (e.g., dietary changes of herbivorous mammalians) that show decreased CO_2 in the atmosphere, which helped drive a vigorous global cooling period [*Cerling et al.*, 1997; *Lyle et al.*, 2008; *Pagani et al.*, 1999]. There is also evidence that between ~7.2 to 5.3 Ma, accelerated cooling of the mid- to high-latitude regions brought SSTs and continental temperature gradients to approximately their modern values [*Herbert et al.*, 2016; *Pound et al.*, 2012]. The absence of sustained enrichment from the marine benthic $\delta^{18}O$ record infers that cooling during the late Miocene did not lead to a large permanent increase in continental ice volume or a decrease in deep-water temperature, suggesting that the polar regions or at least the areas of deep-water formation within the polar oceans were already extremely cold by 8 Ma [*Herbert et al.*, 2016]. From ~5 to ~1.8 Ma, there is some controversy concerning global trends. Some records suggest that in the Pliocene (~4.5-3.2 Ma) there is an increase in mean global temperature, which marks the youngest example of when temperatures were warmer than they are in the modern [*Seki et al.*, 2012]. However, others show that there was a cooling trend by ~4-6°C that occurred from 5 Ma to ~2.5 Ma, preceding the onset of large-amplitude cyclic glaciation in the late Pliocene [*Lear et al.*, 2015]

2.6 Neogene Overturning Circulation and Establishment of the Modern Mode

Compared to the Paleogene, reconstructions of Neogene circulation are relatively unconstrained. There are only a few studies that have attempted to understand the variations of Nd as the global mean temperatures gradually decreased from the Mid-Miocene to the present [*Horikawa et al.*, 2011; *Ling et al.*, 1997; *Martin and Haley*, 2000; *van de Flierdt et al.*, 2004a]. One of the main factors affecting deep-water circulation in the Pacific during this time period was the shoaling of the Panama seaway (20 Ma to ~5-3 Ma) [*Abouchami et al.,* 1997; *Haug and Tiedemann,* 1998]. This restriction cut off direct access of NADW to the Northern Pacific and made AABW the primary deep-water source, increasing the radiogenic signature of Pacific deep-water Nd [*Keigwin,* 1982; *Ling et al.*, 1997]. Equatorial and Southwest Pacific deep-waters indicate that deep-water sourced from the Southern Ocean steadily increased over the Neogene [*van de Flierdt et al.,* 2004a]. Comparison of $\Delta\delta^{13}C$ and Nd isotope data show an increase in vertical mixing within the Pacific water column between 14.3-13.6 Ma; coinciding with ocean-wide improvement in deep-water ventilation and strengthening of the MOC following a large ice-sheet expansion at ~13.8 Ma [*Hodell and Venz-Curtis,* 2006; *Holbourn et al.*, 2013]. Oxygen and carbon isotope comparisons from the Atlantic, Indian, Pacific, and Southern oceans demonstrate that the primary source of deep-water through the middle Miocene was the Southern Ocean, while NADW formation remained weak until ~12.5 Ma [*Holbourn et al.*, 2013; *Woodruff and Savin,* 1989]. The closure of the eastern portal of the Tethys Ocean terminated a source of warm, saline water to the Pacific at ~15 Ma [*Woodruff and Savin,* 1989]. In the Atlantic, Nd isotope data indicates

that the onset of NADW did not occur until 10.6-7.3 Ma [*Thomas and Via*, 2007] coinciding with evidence of Southern Ocean sourced waters in the Caribbean up to 4.6 Ma, followed by an increase in NADW formation and southward movement resulting from increased deep-water ventilation [*Haug and Tiedemann*, 1998]. By 4 Ma, records show that the deep-water of the Pacific Nd signature is less radiogenic than it was previously, which is a result of the increased contribution of NADW to AABW via the ACC [*Ling et al.*, 1997; *Martin and Haley*, 2000].

3. SAMPLES AND METHODS

3.1 IODP Site U1438

IODP Site U1438 (Fig. 3, 4) is in the North Pacific Ocean (27.38351°N, 134.31837°E) at an abyssal water depth of 4720 m. Benthic foraminiferal paleodepth reconstructions [*Arculus et al.*, 2015a] suggest that this site has remained >4000 m through the study interval (30 Ma to the present) and below the carbonate compensation depth (CCD) based on the Pacific-wide CCD reconstruction [*Pälike et al.*, 2012]. The U1438 sedimentary section spans the past ~50-60 Ma [*Arculus et al.*, 2015b; *Arculus et al.*, 2015c]; the age model was constructed with magneto- and biostratigraphy (Fig. 4) [*Arculus et al.*, 2015a]. The material for this study was taken from Cores U1438B-1H to 26X (3 to 217.20 meters below sea floor (mbsf)). This material represents two lithologic units. Unit I (0-160.3 mbsf) is predominately terrigenous and volcaniclastic mud with discrete ash layers and intermittent biogenic ooze layers, and Unit II (160.3-217.20 mbsf) consists of tuffaceous mudstone and fine sandstone that includes moderate to intense deformation. The sedimentation rate for the study interval fluctuated between 1-2 cm/kyr from 0-78 mbsf, then decreased to <1 cm/kyr from 78-174 mbsf, before increasing to 2-4.3 cm/kyr at 174-217 mbsf (Fig. 4).

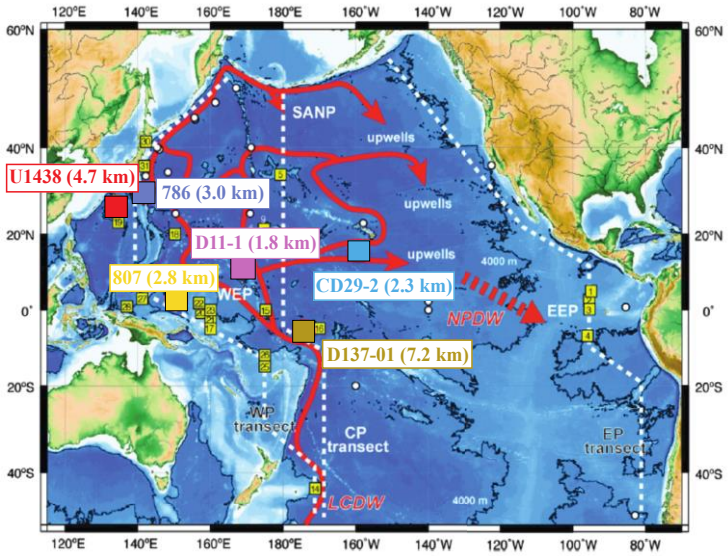

Figure 3. Relevant Pacific Ocean sites in this study. Site 786 and Site 807 from *Martin and Haley* [2000] is at a 3000m water depth and is in the same region as Site U1438. Fe-Mn crust, D11-1 at 1800 m and CD29-2 at 2300 m from *Ling et al.* [1997]. Lastly, Fe-Mn crust, D137-01 at 7200 m from *van de Flierdt et al.* [2004a]. LCDW (red arrows) travels northward maintaining a depth >4000 m, while NPDW (broken red arrow) travels southward across the equator in the eastern Pacific, from *Horikawa et al.* [2011].

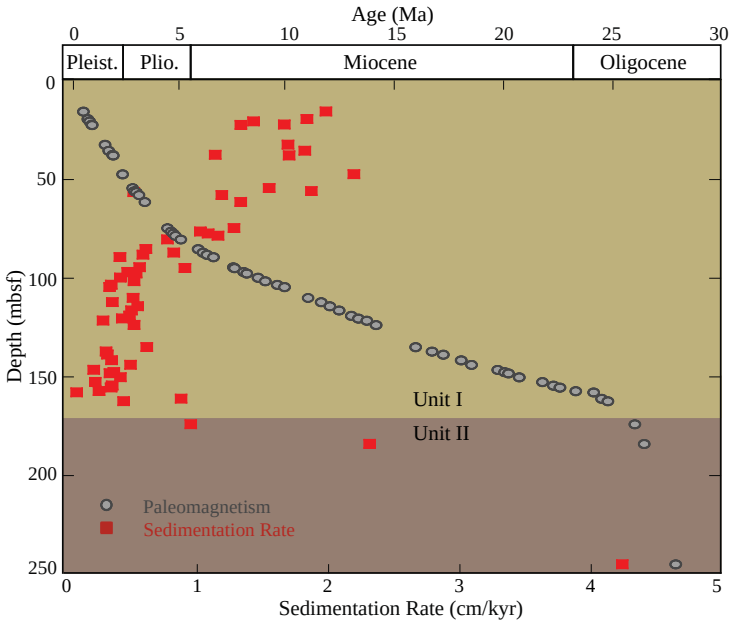

Figure 4. Lithology, sedimentation rate (red squares) and age model (grey circles) based reconstruction of Site U1438. The study interval (0-217.20 mbsf) spans lithologic units I and II, the age model is based on magnetostratigraphic (shown here, grey circles) and biostratigraphic reconstructions [*Arculus et al.* 2015a].

3.2 Analytical Methods

The fossil fish teeth and debris collected from Site U1438 sediment samples were prepared using the general methods of *Basak et al.* [2011] and *Xie et al.* [2012]. To isolate the teeth and debris, bulk sediment was disaggregated and washed through a >63 μm sieve. The sample retained on the sieve was dried overnight in an oven (50°C). For fish teeth/debris analysis, approximately 15-30 apatite specimens per sample were handpicked using a binocular microscope and fine brush. The fragments were then washed three times with ultrapure water (Milli-Q).

For Fe-Mn oxyhydroxide coating analysis, bulk samples were dried overnight and were subsequently pulverized and homogenized with an agate mortar and pestle. These homogenized samples were de-carbonated for 2 h using sodium acetate buffered acetic acid solution that was "pre-cleaned" in cation exchange resin. The remaining material was washed three times with Milli-Q. To reduce the Fe-Mn phases, the oxide fraction was leached in 14 ml of a 0.02 M HH in 20% acetic acid buffered to a pH of 4. The samples with HH solution were placed on a rotary shaker and leached for 2 h. Once the samples were leached they were centrifuged, and the supernatant decanted into a separate clean tube and centrifuged for an additional 1 hour, then decanted and dried. The sample was then digested in concentrated HNO_3 overnight and then placed in 2N HNO_3 for column chemistry. The detrital silicate fraction was taken from the remaining material left behind after the supernatant was decanted. These were placed back in HH for 1.5 h and rinsed 3 times with Milli-Q before being placed for 4 h in HH. Once this

was completed the samples were rinsed 3 times with Milli-Q and dried down over night. The dried sample was homogenized and the material placed in 23 M HF for ~5 days until completely digested. The material was then dried down and placed in concentrated HNO_3-HCL-HNO_3 subsequently before finally being placed in 2N HNO_3 for column chemistry.

All samples (fish teeth/debris, Fe-Mn oxides, and detrital silicates) were then dissolved in 500 μL of 2N HNO_3. The rare earth elements (REE) were isolated using Tru Spec column chemistry (isolating the REE suite from the bulk sample) and the samples collected with 3 ml of 0.05N HNO_3 in Teflon beakers and dried down. The samples were then dissolved in 200 μL of 0.18N HCl and placed on a 100°C hotplate overnight. The Nd fraction was then isolated from the bulk REE via Ln Spec column chemistry by sequentially separating out the bulk REE. Once dried down, the remaining Nd portion was loaded onto a degassed rhenium (Re) filament (0.76 mm width, 25 μm thickness) using 1 μL of 2N HCl and analyzed on a Thermo Scientific Triton thermal ionization mass spectrometer as Nd^+. The ion beams analyzed ranged from 1 to 10 x 10^{-11} A, depending on the amount of Nd loaded and geometry of the double filament assembly, which was not tightly controlled [*Pin et al.*, 2014]. The method used was run in blocks of 16, each block cycled 8 times (collecting individual measurements), a background measurement was run every 2 blocks and the gain was recalibrated after every 5 blocks. External precision was 15 ppm (2σ) with a value of 0.512104 based upon analysis of JNd_i standard through the course of the study. Samples were only used if the absolute

error was $<10^{-6}$. Values higher than this were discarded, apart from 7HCC, 24XCC, and 26XCC – even though the absolute error was $>10^{-6}$ the ε_{Nd} error (<0.5) of these samples were all within acceptable range. Several replicates were run to ensure reproducibility; these were chosen at random throughout the suite of samples. $\varepsilon_{Nd}(t)$ values were calculated using the numerical ship board age models [*Arculus et al.*, 2015]. For the fish teeth/debris $\varepsilon_{Nd}(t)$ ratios a typical $^{147}Sm/^{144}Nd$ value of 0.131, which has been normalized to the bulk earth value and corrected for age (i.e., any in-situ decay of ^{147}Sm once integrated into the biogenic apatite), was applied to all samples in order to correct for any post burial decay of ^{147}Sm after *Thomas et al.* [2008] . A $^{147}Sm/^{144}Nd$ value of 0.109 was used to determine the detrital $\varepsilon_{Nd}(t)$ values established from upper crustal average concentrations of Sm and Nd after *Taylor and McLennan* [1985]. Based on the average Fe-Mn crust values after *Ling et al.* [1997], a $^{147}Sm/^{144}Nd$ value of 0.115 was used for the oxide fraction $\varepsilon_{Nd}(t)$ values.

4. RESULTS

The fish teeth/debris and Fe-Mn oxide data from Site U1438 are presented in Figure 5, Table 1, and Table 2. The record starts at 217.20 mbsf and is highly radiogenic at $\varepsilon_{Nd}(t)$ = -0.2, but is less radiogenic by 193.40 mbsf (-1.4). From 193.40 to 157.05 mbsf there is a shift to less radiogenic values by 2 $\varepsilon_{Nd}(t)$ units and this trend continues, shifting from $\varepsilon_{Nd}(t)$ = -3.4 to -4.9 at 111.97 mbsf. There are two excursions at 127.88 mbsf and 117.55 mbsf, where $\varepsilon_{Nd}(t)$ = -3.5 and -2.6, respectively. The excursion at 117.55 represents a replicate and shows the intra-sample variability (all replicates are shown separately in Figure 5 and then the averages were used when comparing to regional data). The record remains relatively constant from 111.97 mbsf to 83.59 mbsf at around $\varepsilon_{Nd}(t)$ = -4.6 to -4.0. At 79.60 mbsf the record shifts to more radiogenic values ($\varepsilon_{Nd}(t)$ = -3.4), this trend continues until 32.10 mbsf with an excursion at 67.07 mbsf where $\varepsilon_{Nd}(t)$ = -2.6. At 22.60 mbsf the values become less radiogenic (-4.5) and then steadily increase to the top of the sedimentary section (-3.7). The three detrital silicate analyses (Fig. 5, Table 3) were: 148.96 mbsf with a $\varepsilon_{Nd}(t)$ value of -10.7; 127.88 mbsf with a $\varepsilon_{Nd}(t)$ of -3.3; 111.97 mbsf with a $\varepsilon_{Nd}(t)$ value of -11.

Data from fish teeth/debris and Fe-Mn oxide coatings from the same samples (n = 5) were compared to determine how closely the two different phases record the seawater composition at the seafloor (Fig. 6). The comparison has an R^2 value of 0.942, establishing that both types of data represent the Nd record at Site U1438.

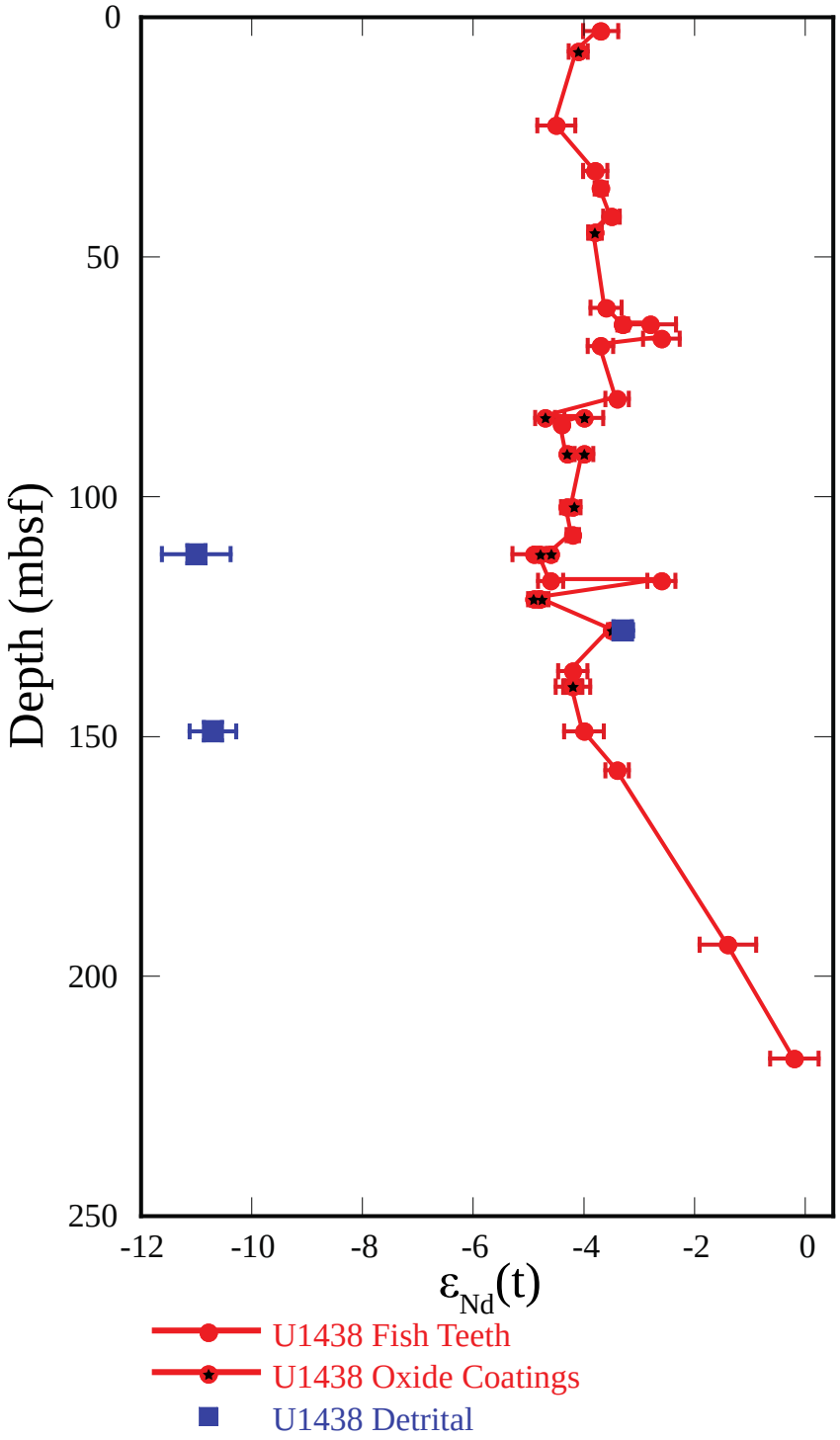

Figure 5. Fish teeth/debris, Fe-Mn oxide coatings, and Detrital $\varepsilon_{Nd}(t)$ values for Site U1438. The data is represented versus depth (m) below seafloor, error bars show the ε_{Nd} error for each specific sample.

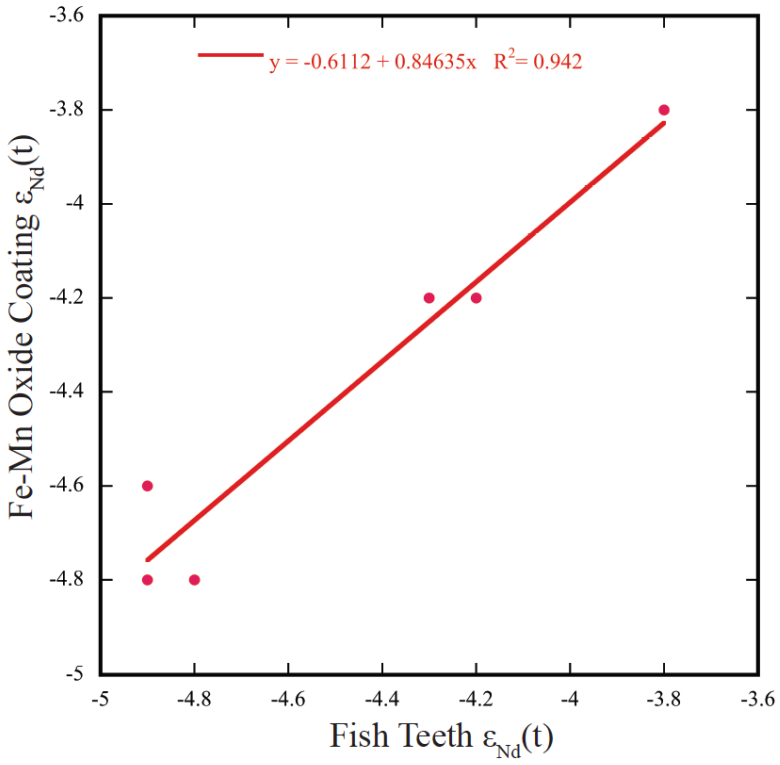

Figure 6. Fish teeth ε_{Nd} values compared to Fe-Mn oxide coatings.

Table 1. Site U1438 Nd isotope data from fossil fish teeth/debris.

Core	Section	Depth (mbsf)	Age (Ma)	$^{143}Nd/^{144}Nd$	Std. Error (abs)	$\varepsilon_{Nd}(t)$
1H	4	2.90	0.15	0.512447	0.000008	-3.7 ± 0.3
3H	4	22.60	1.20	0.512405	0.000009	-4.5 ± 0.3
4H	4	32.10	1.76	0.512445	0.000006	-3.8 ± 0.2
4H	CC	35.73	1.98	0.512443	0.000003	-3.7 ± 0.1
5H	4	41.60	2.32	0.512458	0.000004	-3.5 ± 0.2
5H	CC	44.89	2.47	0.512444	0.000003	-3.8 ± 0.1
7H	4	60.60	3.54	0.512451	0.000007	-3.6 ± 0.3
7H	CC	64.09	3.81	0.512469	0.000002	-3.3 ± 0.1
				0.512491	0.000012	-2.8 ± 0.5
8H	2	67.07	4.05	0.512503	0.000009	-2.6 ± 0.3
8H	3	68.58	4.16	0.512444	0.000006	-3.7 ± 0.2
9H	4	79.60	5.14	0.512461	0.000005	-3.4 ± 0.2
10H	2	85.00	6.00	0.512411	0.000003	-4.4 ± 0.1
11H	7	102.17	9.31	0.512416	0.000003	-4.3 ± 0.1
12H	4	108.05	10.69	0.512417	0.000003	-4.2 ± 0.1
12H	CC	111.97	11.63	0.512384	0.000010	-4.9 ± 0.4
13H	4	117.55	12.73	0.512502	0.000006	-2.6 ± 0.2
				0.512398	0.000006	-4.6 ± 0.2
13H	CC	121.37	13.69	0.512385	0.000004	-4.8 ± 0.2
15H	4	136.42	16.49	0.512417	0.000007	-4.2 ± 0.3
15H	CC	139.64	17.49	0.512415	0.000008	-4.2 ± 0.3
				0.512416	0.000004	-4.2 ± 0.2
16H	CC	148.96	20.40	0.512427	0.000009	-4.0 ± 0.4
17H	5	157.05	23.23	0.512456	0.000005	-3.4 ± 0.2
24X	CC	193.40	26.64	0.512553	0.000013	-1.4 ± 0.5
26X	CC	217.20	27.20	0.512615	0.000011	-0.2 ± 0.4

Table 2. Site U1438 Nd isotope data from Fe-Mn oxyhydroxide coatings.

Core	Section	Depth (mbsf)	Age (Ma)	$^{143}Nd/^{144}Nd$	Std. Error (abs)	$\varepsilon_{Nd}(t)$
1H	CC	7.19	0.36	0.512430	0.000004	-4.1 ± 0.2
5H	CC	44.89	2.47	0.512443	0.000003	-3.8 ± 0.1
9H	CC	83.59	5.77	0.512431	0.000009	-4.0 ± 0.3
				0.512394	0.000005	-4.7 ± 0.2
10H	CC	91.12	7.06	0.512429	0.000004	-4.0 ± 0.2
				0.512413	0.000002	-4.3 ± 0.1
11H	7	102.17	9.31	0.512419	0.000004	-4.2 ± 0.1
12H	CC	111.97	11.63	0.512398	0.000002	-4.6 ± 0.1
				0.512384	0.000003	-4.8 ± 0.1
13H	CC	121.37	13.69	0.512383	0.000002	-4.8 ± 0.1
				0.512378	0.000003	-4.9 ± 0.1
14H	CC	127.88	14.84	0.512452	0.000002	-3.5 ± 0.1
15H	CC	139.64	17.49	0.512412	0.000004	-4.2 ± 0.2
				0.512411	0.000003	-4.2 ± 0.1

Table 3. Site U1438 Nd isotope data from detrital silicates.

Core	Section	Depth (mbsf)	Age (Ma)	$^{143}Nd/^{144}Nd$	Std. Error (abs)	$\varepsilon_{Nd}(t)$
12H	CC	111.97	11.63	0.512070	0.000016	-11.1 ± 0.6
14H	CC	127.88	14.84	0.512459	0.000004	-3.5 ± 0.1
16H	CC	148.96	20.40	0.512077	0.000011	-10.7 ± 0.4

5. DISCUSSION

5.1 U1438 Nd Signature

There are several factors that potentially influence the composition of dissolved Nd at the seafloor in the region of Site U1438. These factors include: (1) contributions of Nd from sediment sources at the seafloor, in the pore waters, or scavenged from surface waters and (2) water mass circulation changes. These need to be considered in order to understand the processes that influence the Nd changes in the U1438 record and if these variations reflect paleoceanographic changes.

As previously stated boundary exchange, where Nd is either released or absorbed, can play a role in the ε_{Nd} values in the region [*Amakawa et al.*, 2009; *Lacan and Jeandel*, 2005; *Ling et al.*, 1997; *Martin and Haley*, 2000]. To a certain extent, the sources contributing to the Nd isotopic composition of deep-water masses are unknown [*Rempfer et al.*, 2012]. The likelihood that the record at Site U1438 is being overprinted by labile sources of volcaniclastic Nd is dependent on how robust the seawater-sediment interaction was in the post-depositional environment. The dissolution of volcanic material from this labile source into the overlying water mass (e.g., NPDW and/or LCDW) potentially introduces additional Nd [*Abbott et al.*, 2015], masking the true Nd isotopic signature and alternatively producing one that is highly radiogenic.

The geographic location of Site U1438 is crucial in determining the origin of the bottom water Nd signature over the past ~27 Ma, as the site's proximity to local volcanism

could make it vulnerable to overprinting. The Kyushu-Palau Ridge (KPR) intersection with the Daito Ridge has volcanic rocks of Eocene age that contain elevated light versus heavy REE ratios [*Arculus et al.*, 2015b]. The unique geochemical characteristic at the KPR/Daito Ridge intersection is thought to be from its involvement of sub-Daito Ridge lithospheric mantle or subarc crust that was metasomatized by a Cretaceous subduction event [*Arculus et al.*, 2015b; *Brandl et al.*, 2017]. The cessation of KPR volcanism was ~25 Ma, followed by the beginning of back-arc spreading of the Shikoku and Parece Vela Basins (i.e., volcanism moved east of the KPR) [*Ishizuka et al.*, 2011].

Oceanic pore fluid profiles indicate that a large portion of Nd to the oceans, which is unaccounted for, could be a benthic flux of Nd from sedimentary pore fluids [*Abbott et al.*, 2015]. Site U1438 is in a prime location to have long exposure times to a benthic flux due to slow deep-water renewal in the North Pacific. *Abbott et al.* [2015] shows that marine sediments are the dominant benthic source of Nd to the oceans and that the ε_{Nd} of deep-water within the Pacific basin is controlled largely by this benthic source. Having a long exposure time to a benthic flux (e.g., volcanic material) can alter the ε_{Nd} of the bottom water, a possible cause for the higher radiogenic record at Site U1438 from 27.20 to 16.49 Ma. *Arculus et al.* [2015a] shows that Ca and Mg at U1438 exhibited opposite trends from 3 to 298 mbsf, where Ca increased linearly at a high rate while Mg concentrations decreased linearly over the same depth. This synchronous increase in Ca and decrease in Mg is attributed to the diagenesis of volcaniclastic sediments [*Arculus et al.*, 2015a]. The observed trend is contrary to many cases where there is not an increase

in concentration after burial due to the limited amount of REE within the pore waters [*Staudigel et al.*, 1985]. For example, *Molina-Kescher et al.* [2014] found that "boundary exchange" does not necessarily play a significant role in the bottom water Nd isotope composition of certain regions (e.g., the western South Pacific).

A way to determine the role of pore water and particle contribution of ε_{Nd} to the bottom water (i.e., the legitimacy of the water mass $\varepsilon_{Nd}(t)$ signature in fish/debris and Fe-Mn oxide coatings) at a given location is to analyze the detrital silicate component. For locations near land, the detrital component will most likely represent the regional weathering inputs delivered to the surface at that location. Since this is the case and the Nd isotopic composition of terrigenous inputs is analogous to the oceanic surface waters [*Goldstein and Jacobsen*, 1987], the resulting detrital value can be compared to the value recorded by fish debris. The detrital silicate component at Site U1438 shows large variation in the three samples that were analyzed. The extreme shift at 127.88 mbsf (14.84 Ma) to a highly radiogenic value compared to the other two other silicate samples can potentially be explained by the large amount of volcaniclastic material mixed in with detrital silicates (mainly composed of volcanic material; e.g., pyroclastics) found within that sample (Fig. 7). The remaining two silicate records reflect an extremely unradiogenic signal when compared to the fish teeth/debris and oxide coatings. With the difference between the detrital silicates and the fish teeth/debris and Fe-Mn oxide coatings it is evident that the fish teeth/debris and coatings are most likely reflecting a signal that has not been influenced by any local dissolved Nd inputs apart from an outlier

at 12.73 Ma that has potentially been overprinted by the volcanic content of the detrital fraction.

Site 786A and Site 807A are in the North Pacific (Fig. 8), like Site U1438, and were cored near the Izu-Bonin-Mariana Arc with sediments made up primarily of nannofossil marls and clays with persistent volcanogenic material throughout [*Martin and Haley,* 2000]. *Martin and Haley* [2000] suggest that the values recorded at 786A by the fish teeth reflect a unique water mass composition. Although the fish teeth records from 786A and 807A at times are slightly higher than the Fe-Mn crust data, an opposite trend to what is expected based on water depths since these sites are from a greater modern depth, if they were not overprinted the Nd values should be slightly less radiogenic [*Martin and Haley,* 2000; *Piepgras and Wasserburg,* 1987]. The slightly higher radiogenic Nd values from the fish teeth infers that there is influence from a local source of dissolved Nd. *Martin and Haley* [2000] say the signature is sourced from the underlying volcaniclastic sediment and basaltic basement. The fish teeth are subsequently recording the signature of the fluids released by dissolution of labile volcanic material into the local bottom water at the time of deposition. They also point out that radiogenic values could be caused by alteration as a consequence of pore water exposure during burial and the diagenesis of local volcanic material [*Martin and Haley*, 2000]. As seen at 786A and 807A, at U1438 the record is consistently more radiogenic prior to 13.69 Ma than both the Fe-Mn crusts records from D11-1 and CD29-2. Bearing in mind the lithology of this interval (~23.5 Ma, Fig 8) and the overall trends of Ca and

Mg, it is very possible that the volcaniclastic mud, tuffaceous mud, and ash layers contributed additional Nd to the surrounding bottom waters, thereby driving the more radiogenic signature in the U1438 fish teeth record.

Similarities between Sites 786A and U1438 support the idea that there was a potential influence from volcanic material prior to ~14 Ma because the patterns are consistent; once the volcanism ceases and the lithology changes from tuffaceous material to volcaniclastic material their values decrease (they are extremely radiogenic prior to this shift) to reflect similar records to other regional data. At U1438, the upper portion of the record (i.e., 14-0 Ma) shows that once the prolific phase of volcanic activity began to decrease the record indicates a lower contribution of radiogenic Nd. However, the background volcanism, as the Shikoku and Parece Vela Basins opened during the Neogene, produce a strong potential to influence the concentrations of radiogenic Nd within the sediment. This potential is evident in the records of U1438, 786A, and 807A since they all have several instances that are extremely more radiogenic than the other contemporaneous records.

Figure 7. Site U1438 – 14HCC (127.88 mbsf). Note the abundance of volcaniclastic material (see red arrows) in the field of view. Image taken from a dissecting microscope X10 magnification.

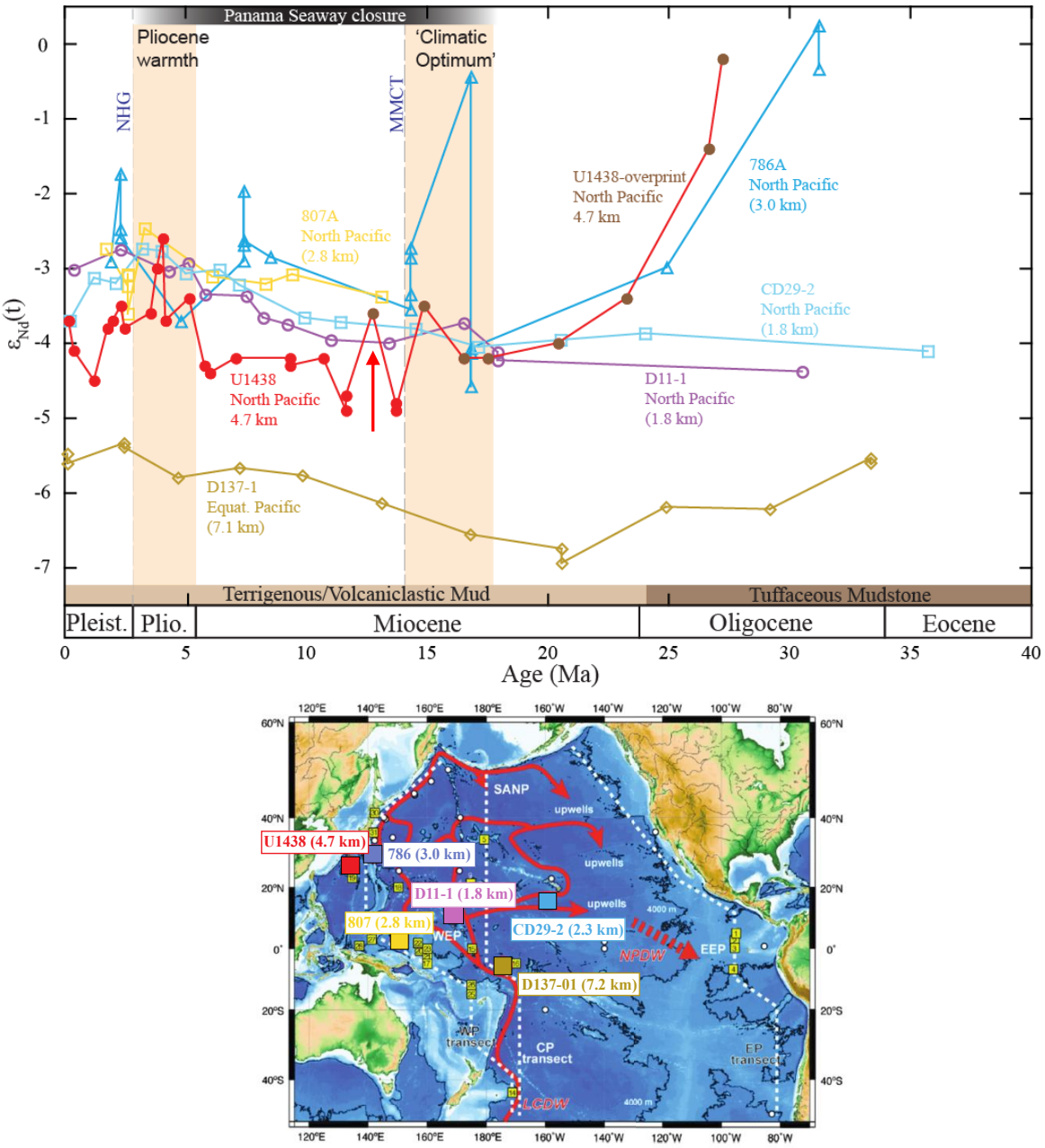

Figure 8. Compilation of new data (Site U1438) and existing data. From *Ling et al.* [1997], crust CD29-2, D11-1; from *Martin and Haley* [2000], Site 786A and 807A; and from *van de Flierdt et al.* [2004a], crust D137-01. The relevant climatic and geologic events are overlaid for context. The lower section of U1438 that is thought to be overprinted is indicated by solid brown circles with the data point beyond the continued overprinting indicated by a red arrow. The lithological representation is of the U1438 change in lithology at 160.3 mbsf. 0-160.3 mbsf is terrigenous and volcaniclastic mud with ash layers throughout and 160.3-257.13 mbsf consist of tuffaceous mudstone and fine sandstone. The map shows the present geographic location of each record.

5.2 Regional Comparison

Previously published data from the region spanning a similar time interval to the new U1438 record include a compilation of both fish teeth (Sites 786A and 807A) and Fe-Mn crust (D11-1, CD29-2, and D137-01) Nd records (Fig. 8). These North Pacific sites situated at intermediate- and deep-water depths exhibit relatively higher radiogenic values over the past 27 Ma, with averages from -4 to -3. Additionally, DC137-01 in the Equatorial Pacific is the most impacted by CDW today, and shows the least radiogenic values over the last 27 Ma ranging from -6.5 to -5.5 [*van de Flierdt et al.,* 2004a].

Once the record seems to show a relative decrease in overprinting there is a large peak (e.g., -3.6 at 12.73 Ma; Fig. 8 red arrow) that may have resulted from the dispersed ash layers and disseminated ash (caused by bioturbation of pre-existing layers, the settling of air-born ash, spreading from subaqueous eruptions, and other mechanisms; e.g., *Scudder et al.* [2016]); although, this outlier does not affect the overall trend from 14-0 Ma. Based on the large separation between the recorded ash layers (samples for this study avoid any ash layers; Fig. 9) [*Arculus et al.,* 2015a] and the excursions seen within in the record it is likely that disseminated ash had a larger role in the record after ~14 Ma.

Site U1438 and D11-1 (Fig. 8) become slightly more radiogenic producing a small peak around 7 Ma and then fall back to less radiogenic before they shift to even more radiogenic values by ~1 epsilon unit, maintaining this trend into the present. This shift is a potential result of the initial restriction and ultimately the final closure to the

Panamanian seaway deep-water passage, restricting the influence of NADW (ε_{Nd} = ~-13) to the deep-water of the northern Pacific and directly influencing the ε_{Nd} values, causing them to become more radiogenic [*Keigwin*, 1982; *Ling et al.*, 1997]. The Fe-Mn crust record at D137-01, the southernmost record located in the equatorial Pacific is extremely remote making it very unlikely bottom water at this location is influenced by any erosional inputs from volcanism or continental influences, shows the enhanced CDW flux since ~14 Ma from the Southern Ocean reflecting the mixture of AABW (ε_{Nd} = ~-9; e.g., *Stichel et al.* [2012]) and equatorial Pacific deep-water [*van de Flierdt et al.*, 2004].

With the Nd intermediate and deep-water signal relatively constrained by these sites, the signal at Site U1438 supports that deep-water in the Northwestern Pacific switched from NPDW to being bathed predominately in LCDW by at least 14 Ma. From 14 Ma to ~4 Ma the $\varepsilon_{Nd}(t)$ signal at U1438 remains slightly less radiogenic than the other regional records, but more radiogenic than the Central Pacific record (D137-01), indicating continued coverage of LCDW through this time. Climatic changes and tectonic changes (e.g., closure of the Panama Seaway and restriction of the Indonesian Throughflow) affecting water mass circulation also have to be considered as possible influences to the Nd signature at Site U1438. Based on *Thomas* [2004] who showed that in general as the $\delta^{18}O$ signature (lower $\delta^{18}O$ indicates warmer temperatures) increased the $\varepsilon_{Nd}(t)$ values became less radiogenic. The Nd regional deep-water variations through time as the

Miocene progressed could very well be caused by the beginning of the observed global cooling trend. Although evidence of volcanic activity before 14 Ma could indicate that the record may be overprinted, the more radiogenic Nd values from 27.20 to 13.69 Ma could also be consistent with an increase in the amount of the more radiogenic NDPW (e.g., the Paleogene mode), directly coinciding with the warmer climate of the early Miocene. The shift seen at Site 786A at ~15 Ma, where the record becomes less radiogenic, does support this interpretation at Site U1438, although the authors do not directly mention a change in water mass coverage [*Martin and Haley*, 2000] Once the MMCO ceases and the overall gradual decrease in global temperatures begins the Nd record shifts to less radiogenic (e.g., ~0 to ~-4) by ~14 Ma, and becomes completely bathed in LCDW (e.g., the modern mode). This could possibly be caused by the cooling of Pacific bottom water, as well as increased equator-to-pole thermal and temperature gradients caused by the decreasing temperatures. It is possible that these decreasing temperatures along with the gradual closure of the Panama seaway resulted in a more vigorous CDW formation due to increased sea ice formation (i.e., increased brine rejection) in the Antarctic and an increase in CDW pushing further northward [*Holbourn et al.*, 2013; *Lear et al.*, 2015; *van de Flierdt et al.*, 2004a], aiding in the observed shift from the Paleogene mode to the modern mode at ~14 Ma. While the final closure of the seaway and the increasing influence of NADW to AABW is seen around 4 Ma when the record shift slightly back to -3 coinciding with the Pliocene warming period (the last recorded period, where temperatures are warmer than the modern) [*Seki et al.*, 2012].

Site 807A in Northwestern Pacific agrees with Site 786A in the earlier portion of the record (0-13.1 Ma), indicating a decreasing trend to modern ε_{Nd} values as the volcanic material becomes less abundant [*Martin and Haley*, 2000]. Both records along with U1438 remain relatively constant after they settle at ~-4 from ~13-14 Ma until ~5 Ma. The inferred increased temperatures of the Pliocene (~5 Ma) coincides with the radiogenic $\varepsilon_{Nd}(t)$ increase at Site U1438 from -4.4 to -3.4 before hitting a peak at ~4 Ma ($\varepsilon_{Nd}(t) = -2.6$), and a notable increase in the Nd record at 807A (-3.16 to -2.5). The Nd signature at U1438 and 786A as well as the temperature decreases again with the onset of Northern Hemispheric Glaciation. With the climate variations so closely mirroring the Nd isotopic flux at U1438, it is plausible that with the changes from warm to cold temperatures there is also a shift in deep-water sources (e.g., Pacific northern high latitudes during warming periods and Southern Ocean sourced deep-water during cooling periods) [*Thomas*, 2004].

At 4 Ma the $\varepsilon_{Nd}(t)$ values shift to less radiogenic implying a stronger NADW influence on the Southern Ocean sourced LCDW, a shift that is also reflected in the Fe-Mn crust records of CD29-2, Sites 786A, and 807A. The regional records including Site U1438 support a southern sourced deep-water mass, while U1438 demonstrates the expected deviation from other the Fe-Mn crust records by remaining less radiogenic, unlike 786A and 807A, inferring that U1438 has less overprinting of its Nd signature from local input and is recording an accurate CDW signature.

Overall, present-day distribution and time-series data show variations in the Nd isotope values of deep and bottom water are smaller than latitudinal or vertical differences, which maintains that the Pacific Ocean circulation has been similar back to the Oligocene [*Frank*, 2002; *Talley*, 2013; *van de Flierdt et al.*, 2004a]. However, *Horikawa et al.* [2011] showed that the behavior of Nd throughout different regions of the Pacific varied drastically based on local sources of Nd. This is evident from the previous data as well as U1438, since the fish teeth differ from regional Fe-Mn crust Nd signatures.

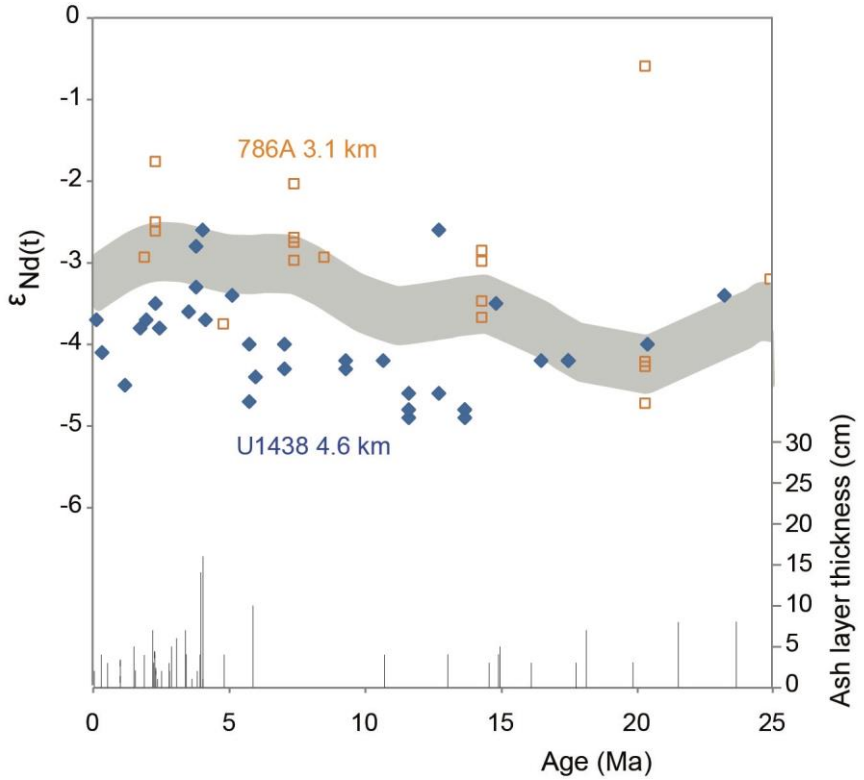

Figure 9. The $\varepsilon_{Nd(t)}$ values of Sites U1438 and 786A from *Kender et al.* [in review]. This is compared with the North Pacific intermediate water average (highlighted in grey). Also shown are ash layers. Also, it is important to note none of the samples from U1438 were taken directly from ash layers.

5.3 Site U1438 Global Implications

Within the Site U1438 Nd record the paleoceanographic signal indicates that between ~27-14 Ma the Northwest Pacific was bathed in NPDW as opposed to ~14-0 Ma where it is bathed in CDW, although there is a strong possibility for water mass overprinting in several sectors (e.g., >14 Ma). The Nd record at U1438 shows that CDW began to bathe the region as the deep-water of the Northern Pacific cooled and the formation of NDPW weakened. The amount of CDW to U1438 increases after 14 Ma, which implies that the formation of CDW in the Southern Ocean increased due to global temperatures decreasing resulting in an increase of oceanic gradients forcing CDW northward [*Herbert et al.,* 2016; *Pound et al.,* 2012]. Additionally, the final decrease of NPDW at U1438 is supported by the Indo-Pacific Seaway closure, while the increase of CDW is supported by the formation of the EAIS causing increased ventilation that resulted in a strong MOC within the Pacific contributing to the northward movement of CDW [*Hodell and Venz-Curtis*, 2006; *Holbourn et al.*, 2013; *Holbourn et al.*, 2014; *Romine and Lombari*, 1985; *Woodruff and Savin,* 1989]. U1438 shows an increase to the radiogenic signature of Nd within the Pacific deep-water as the influence of NADW to the Pacific steadily decreased with the gradual closure of the Panama Seaway beginning at 20 Ma [*Abouchami et al.,* 1997; *Haug and Tiedemann*, 1998]. As global temperatures cooled and U1438 becomes fully bathed by CDW the formation of NADW within the Atlantic became more vigorous forcing the water mass southward to be mixed with AABW [*Haug and Tiedemann,* 1998]. U1438 and 786A seemingly shift to a less radiogenic Nd signature as NADW is introduced back into the Pacific by mixing with

AABW. The change from the Paleogene mode to the modern mode, as determined by the record at U1438, appears completed by 14 Ma, coinciding with the end of the MMCO and the overall global cooling trends within the Neogene. Once the modern mode of circulation begins to influence the Pacific U1438 remains bathed in CDW into the present.

6. CONCLUSION

The goal of this study was to reconstruct deep-water circulation within the North Pacific to help determine when the mode of circulation switched between the Paleogene mode and the modern mode. IODP Site U1438, located in the Northwestern Pacific, created the opportunity to constrain this shift. U1438 had two potential aspects that influenced the Nd record during the Neogene, the local volcanism and the change in water mass circulation patterns. Prior to 14 Ma, much of the record is seemingly affected by the local volcanism as it shows an extremely radiogenic Nd signature that is much higher than regional Fe-Mn crust records. Although, the signature helped in determining that NPDW did bathe the deep-water site during this time it does not truly represent a paleoceanographic signal. While after 14 Ma the Nd record drops to a less radiogenic signature compared to the Fe-Mn records and more closely resembles the signature of the southern sourced LCDW. The tectonic activity (e.g., the closure of the Panama Seaway) and the climatic cooling that occurred during the Neogene contributed a large amount to introducing LCDW to the Northern Pacific. Additionally, the formation of the EAIS increased the amount of LCDW being pushed northward and the onset of Northern Hemispheric glaciation aided in pushing NADW southward to CDW, ultimately forming the modern GOC.

The Nd isotopic record collected at U1438 showed that the change between the Paleogene mode to the modern mode occurred by 14 Ma, coinciding with the large shift in climate from a relatively warm world to a gradually cooling world that was

established by the end of the MMCO, also supported by trends observed at Site 786. Even though the switch between the Paleogene mode and modern mode of circulation is clearly evident from Site U1438, the contribution of additional sources of Nd is something that must not be ignored. There was clear overprinting on the lower portion of the record, as the Fe-Mn crust are far less radiogenic than U1438 (e.g., >14 Ma), from local volcanic activity that masked the true paleoceanographic signal. This must be considered when adding new Nd circulation reconstructions to the overall global circulation reconstruction.

REFERENCES

Abbott, A. N., B. A. Haley, and J. McManus (2015), Bottoms up: Sedimentary control of the deep North Pacific Ocean's εNd signature, *Geology*, *43*(11), 1035-1035, doi:10.1130/g37114.1.

Abbott, A. N., B. A. Haley, A. K. Tripati, and M. Frank (2016), Constraints on ocean circulation at the Paleocene–Eocene Thermal Maximum from neodymium isotopes, *Clim. Past*, *12*(4), 837-847, doi:10.5194/cp-12-837-2016.

Abouchami, W., S. L. Goldstein, S. J. G. Gazer, A. Eisenhauer, and A. Mangini (1997), Secular changes of lead and neodymium in central Pacific seawater recorded by a Fe-Mn crust, *Geochimica et Cosmochimica Acta*, 61(18), 3957-3974, doi:http://dx.doi.org/10.1016/S0016-7037(97)00218-4.

Amakawa, H., Y. Nozaki, D. S. Alibo, J. Zhang, K. Fukugawa, and H. Nagai (2004), Neodymium isotopic variations in Northwest Pacific waters, *Geochimica et Cosmochimica Acta*, *68*(4), 715-727, doi:http://dx.doi.org/10.1016/S0016-7037(03)00501-5.

Amakawa, H., K. Sasaki, and M. Ebihara (2009), Nd isotopic composition in the central North Pacific, *Geochimica et Cosmochimica Acta*, *73*(16), 4705-4719, doi:http://dx.doi.org/10.1016/j.gca.2009.05.058.

Arculus, R. J., et al. (2015a), Site U1438. In Arculus, R.J., Ishizuka, O., Bogus, K., and the Expedition 351 Scientists, Proceedings of the International Ocean Discovery Program, Expedition 351: Izu-Bonin-Mariana Arc Origins*Rep.*, College Station, TX (International Ocean Discovery Program).

Arculus, R. J., O. Ishizuka, K. Bogus, and E. Scientists (2015b), Proceedings of the International Ocean Discovery Program, Expedition 351: Izu-Bonin-Mariana Arc Origins*Rep.*, College Station, TX (International Ocean Discovery Program).

Arculus, R. J., et al. (2015c), A record of spontaneous subduction initiation in the Izu-Bonin-Mariana arc, *Nature Geosci*, *8*(9), 728-733, doi:10.1038/ngeo2515 http://www.nature.com/ngeo/journal/v8/n9/abs/ngeo2515.html - supplementary-information.

Arsouze, T., J. C. Dutay, F. Lacan, and C. Jeandel (2009), Reconstructing the Nd oceanic cycle using a coupled dynamical – biogeochemical model, *Biogeosciences*, *6*(12), 2829-2846, doi:10.5194/bg-6-2829-2009.

Basak, C., E. E. Martin, and G. D. Kamenov (2011), Seawater Pb isotopes extracted from Cenozoic marine sediments, *Chemical Geology*, *286*(3), 94-108.

Brandl, P.A., et al. (2017), The arc arises: The links between volcanic output, arc evolution and melt composition, *Earth and Planetary Science Letters*, 461, 73-84, doi:http://dx.doi.org/10.1016/j.epsl.2016.12.027.

Broecker, W. S. (2010), *The great ocean conveyor : discovering the trigger for abrupt climate change*, Princeton: Princeton University Press.

Broecker, W. S., R. Gerard, M. Ewing, and B. C. Heezen (1960), Natural radiocarbon in the Atlantic Ocean, *Journal of Geophysical Research*, *65*(9), 2903-2931, doi:10.1029/JZ065i009p02903.

Carter, P., D. Vance, C. D. Hillenbrand, J. A. Smith, and D. R. Shoosmith (2012), The neodymium isotopic composition of waters masses in the eastern Pacific sector of the Southern Ocean, *Geochimica et Cosmochimica Acta*, *79*(0), 41-59, doi:http://dx.doi.org/10.1016/j.gca.2011.11.034.

Cerling, T. E., J. M. Harris, B. J. MacFadden, M. G. Leakey, J. Quade, V. Eisenmann, and J. R. Ehleringer (1997), Global vegetation change through the Miocene/Pliocene boundary, *Nature*, *389*(6647), 153-158.

DePaolo, D. J., and G. J. Wasserburg (1976), Nd isotopic variations and petrogenetic models, *Geophys. Res. Lett.*, *3*(5), 249-252, doi:10.1029/GL003i005p00249.

Elderfield, H., and M. J. Greaves (1982), The rare earth elements in seawater, *Nature*, *296*(5854), 214-219.

Elderfield, H., and E. R. Sholkovitz (1987), Rare earth elements in the pore waters of reducing nearshore sediments, *Earth and Planetary Science Letters*, *82*(3), 280-288, doi:http://dx.doi.org/10.1016/0012-821X(87)90202-0.

Elderfield, H., M. Whitfield, J. D. Burton, M. P. Bacon, and P. S. Liss (1988), The Oceanic Chemistry of the Rare-Earth Elements [and Discussion], *Philosophical Transactions of the Royal Society of London. Series A, Mathematical and Physical Sciences*, *325*(1583), 105-126, doi:10.1098/rsta.1988.0046.

Faure, G., and T. M. Mensing (2005), *Isotopes: principles and applications. 3rd ed*, John Wiley & Songs, Inc., Hoboken, N.J.

Frakes, L. A., and E. M. Kemp (1972), Influence of Continental Positions on Early Tertiary Climates, *Nature*, *240*(5376), 97-100.

Frank, M. (2002), Radiogenic Isotopes: Tracers of Past Ocean Circulation and Erosional Input, *Reviews of Geophysics*, *40*(1), 1-1-1-38, doi:10.1029/2000RG000094.

Goldstein, S., and S. R. Hemming (2003), Long-lived Isotopic Tracers in Oceanography, Paleoceanography, and Ice-sheet Dynamics, in *Treatise on Geochemistry*, edited by E. Ltd., 453-489, Elsevier Ltd.

Goldstein, S., and S. B. Jacobsen (1987), The Nd and Sr isotopic systematics of river-water dissolved material: Implications for the sources of Nd and Sr in seawater, *Chemical Geology: Isotope Geoscience section*, *66*(3-4), 245-272, doi:10.1016/0168-9622(87)90045-5.

Goldstein, S., and R. K. O'Nions (1981), Nd and Sr isotopic relationships in pelagic clays and ferromanganese deposits, *Nature*, *292*(5821), 324-327, doi:10.1038/292324a0.

Gregory, J. M. (2000), Vertical heat transports in the ocean and their effect on time-dependent climate change, *Climate Dynamics*, *16*(7), 501-515, doi:10.1007/s003820000059.

Gregory, J. M., et al. (2005), A model intercomparison of changes in the Atlantic thermohaline circulation in response to increasing atmospheric CO_2 concentration, *Geophysical Research Letters*, *32*(12), 5, doi:10.1029/2005gl023209.

Hague, A. M., D. J. Thomas, M. Huber, R. Korty, S. C. Woodard, and L. B. Jones (2012), Convection of North Pacific deep water during the early Cenozoic, *Geology*, *40*(6), 527-530, doi:10.1130/g32886.1.

Haug, G. H., and R. Tiedemann (1998), Effect of the formation of the Isthmus of Panama on Atlantic Ocean thermohaline circulation, *Nature*, *393*(6686), 673-676.

Halliday, A. N., J. P. Davidson, P. Holden, R. M. Owen, and A. M. Olivarez (1992), Metalliferous sediments and the scavenging residence time of Nd near hydrothermal vents, *Geophys. Res. Lett.*, *19*(8), 761-764, doi:10.1029/92gl00393.

Herbert, T. D., K. T. Lawrence, A. Tzanova, L. C. Peterson, R. Caballero-Gill, and C. S. Kelly (2016), Late Miocene global cooling and the rise of modern ecosystems, *Nature Geosci*, *9*(11), 843-847, doi:10.1038/ngeo2813 http://www.nature.com/ngeo/journal/v9/n11/abs/ngeo2813.html - supplementary-information.

Holbourn, A., W. Kuhnt, M. Frank, and B. A. Haley (2013a), Changes in Pacific Ocean circulation following the Miocene onset of permanent Antarctic ice cover, *Earth and Planetary Science Letters*, *365*, 38-50, doi:http://dx.doi.org/10.1016/j.epsl.2013.01.020.

Holbourn, A., W. Kuhnt, K. G. D. Kochhann, N. Andersen, and K. J. S. Meier (2015), Global perturbation of the carbon cycle at the onset of the Miocene Climatic Optimum, *Geology*, doi:10.1130/g36317.1.

Holbourn, A., W. Kuhnt, M. Lyle, L. Schneider, O. Romero, and N. Andersen (2013b), Middle Miocene climate cooling linked to intensification of eastern equatorial Pacific upwelling, *Geology*, doi:10.1130/g34890.1.

Hollis, C. J., et al. (2009), Tropical sea temperatures in the high-latitude South Pacific during the Eocene, *Geology*, *37*(2), 99-102, doi:10.1130/g25200a.1.

Horikawa, K., E. E. Martin, Y. Asahara, and T. Sagawa (2011), Limits on conservative behavior of Nd isotopes in seawater assessed from analysis of fish teeth from Pacific core tops, *Earth and Planetary Science Letters*, *310*(1–2), 119-130, doi:http://dx.doi.org/10.1016/j.epsl.2011.07.018.

Ingri, J., A. Widerlund, M. Land, Ö. Gustafsson, P. Andersson, and B. Öhlander (2000), Temporal variations in the fractionation of the rare earth elements in a boreal river; the role of colloidal particles, *Chemical Geology, 166*, 23-45, doi:10.1016/S0009-2541(99)00178-3.

Jones, C. E., A. N. Halliday, D. K. Rea, and R. M. Owen (1994), Neodymium isotopic variations in North Pacific modern silicate sediment and the insignificance of detrital REE contributions to seawater, *Earth and Planetary Science Letters*, *127*(1-4), 55-66, doi:10.1016/0012-821x(94)90197-x.

Keigwin, L. (1982), Isotopic Paleoceanography of the Caribbean and East Pacific: Role of Panama Uplift in Late Neogene Time, edited, 350, The American Association for the Advancement of Science.

Kender, S., et al. (in review), Increased Circumpolar Deep Water flux to the North Pacific during the mid-Miocene climate transition, *Geology*.

Kennett, J. P., G. Keller, and M. S. Srinivasan (1985), Miocene planktonic foraminiferal biogeography and paleoceanographic development of the Indo-Pacific region, *Geological Society of America Memoirs*, *163*, 197-236, doi:10.1130/MEM163-p197.

Lacan, F., and C. Jeandel (2001), Tracing Papua New Guinea imprint on the central Equatorial Pacific Ocean using neodymium isotopic compositions and Rare Earth Element patterns, *Earth and Planetary Science Letters*, *186*(3-4), 497-512, doi:http://dx.doi.org/10.1016/S0012-821X(01)00263-1.

Lacan, F., and C. Jeandel (2004), Neodymium isotopic composition and rare earth element concentrations in the deep and intermediate Nordic Seas: Constraints on the Iceland Scotland Overflow Water signature, *Geochemistry, Geophysics, Geosystems*, *5*(11), doi:10.1029/2004GC000742.

Lacan, F., and C. Jeandel (2005), Neodymium isotopes as a new tool for quantifying exchange fluxes at the continent–ocean interface, *Earth and Planetary Science Letters*, *232*(3-4), 245-257, doi:http://dx.doi.org/10.1016/j.epsl.2005.01.004.

Lacan, F., K. Tachikawa, and C. Jeandel (2012), Neodymium isotopic composition of the oceans: A compilation of seawater data, *Chemical geology*.

Lambelet, M., T. van de Flierdt, K. Crocket, M. Rehkämper, K. Kreissig, B. Coles, M. J. A. Rijkenberg, L. J. A. Gerringa, H. J. W. de Baar, and R. Steinfeldt (2016), Neodymium isotopic composition and concentration in the western North Atlantic Ocean: Results from the GEOTRACES GA02 section, *Geochimica et Cosmochimica Acta*, *177*, 1-29, doi:http://dx.doi.org/10.1016/j.gca.2015.12.019.

Lear, C. H., H. K. Coxall, G. L. Foster, D. J. Lunt, E. M. Mawbey, Y. Rosenthal, S. M. Sosdian, E. Thomas, and P. A. Wilson (2015), Neogene ice volume and ocean temperatures: Insights from infaunal foraminiferal Mg/Ca paleothermometry, *Paleoceanography*, *30*(11), 1437-1454, doi:10.1002/2015PA002833.

Ling, H. F., K. W. Burton, R. K. O'Nions, B. S. Kamber, F. von Blanckenburg, A. J. Gibb, and J. R. Hein (1997), Evolution of Nd and Pb isotopes in Central Pacific seawater from ferromanganese crusts, *Earth and Planetary Science Letters*, *146*(1–2), 1-12, doi:http://dx.doi.org/10.1016/S0012-821X(96)00224-5.

Lyle, M., J. Barron, T. J. Bralower, M. Huber, A. Olivarez Lyle, A. C. Ravelo, D. K. Rea, and P. A. Wilson (2008), Pacific Ocean and Cenozoic evolution of climate, *Reviews of Geophysics*, *46*(2), doi:10.1029/2005RG000190.

Martin, E. E., and B. A. Haley (2000), Fossil fish teeth as proxies for seawater Sr and Nd isotopes, *Geochimica et Cosmochimica Acta*, *64*(5), 835-847, doi:http://dx.doi.org/10.1016/S0016-7037(99)00376-2.

Molina-Kescher, M., M. Frank, and E. C. Hathorne (2014), Nd and Sr isotope compositions of different phases of surface sediments in the South Pacific: Extraction of seawater signatures, boundary exchange, and detrital/dust provenance, *Geochemistry, Geophysics, Geosystems*, *15*(9), 3502-3520, doi:10.1002/2014GC005443.

Orsi, A. H., G. C. Johnson, and J. L. Bullister (1999), Circulation, mixing, and production of Antarctic Bottom Water, *Progress in Oceanography*, *43*(1), 55-109, doi:http://dx.doi.org/10.1016/S0079-6611(99)00004-X.

Pagani, M., M. A. Arthur, and K. H. Freeman (1999), Miocene evolution of atmospheric carbon dioxide, *Paleoceanography*, *14*(3), 273-292, doi:10.1029/1999PA900006.

Pälike, H., et al. (2012), A Cenozoic record of the equatorial Pacific carbonate compensation depth, *Nature*, *488*(7413), 609-614, doi:http://www.nature.com/nature/journal/v488/n7413/abs/nature11360.html - supplementary-information.

Park, T. W., Y. Deng, M. Cai, J. H. Jeong, and R. J. Zhou (2014), A dissection of the surface temperature biases in the Community Earth System Model, *Climate Dynamics*, *43*(7-8), 2043-2059, doi:10.1007/s00382-013-2029-9.

Pearson, P. N., P. W. Ditchfield, J. Singano, K. G. Harcourt-Brown, C. J. Nicholas, R. K. Olsson, N. J. Shackleton, and M. A. Hall (2001), Warm tropical sea surface temperatures in the Late Cretaceous and Eocene epochs, *Nature*, *413*(6855), 481-487, doi:http://www.nature.com/nature/journal/v413/n6855/suppinfo/413481a0_S1.html.

Piepgras, D. J., and S. B. Jacobsen (1988), The isotopic composition of neodymium in the North Pacific, *Geochimica et Cosmochimica Acta*, *52*(6), 1373-1381, doi:http://dx.doi.org/10.1016/0016-7037(88)90208-6.

Piepgras, D. J., and G. J. Wasserburg (1982), Isotopic composition of neodymium in waters from the Drake Passage, *Science*, *217*, 207-214.

Piepgras, D. J., and G. J. Wasserburg (1987), Rare earth element transport in the western North Atlantic inferred from Nd isotopic observations, *Geochimica et Cosmochimica Acta*, *51*(5), 1257-1271, doi:10.1016/0016-7037(87)90217-1.

Pin, C., A. Dupont, and A. Gannoun (2014), Rapid, simultaneous separation of Sr, Pb, and Nd by extraction chromatography prior to isotope ratios determination by TIMS and MC-ICP-MS, *Journal of Analytical Atomic Spectrometry*, *29*(10), 1858-1870, doi:10.1039/c4ja00169a.

Rempfer, J., T. F. Stocker, F. Joos, and J.-C. Dutay (2012), Sensitivity of Nd isotopic composition in seawater to changes in Nd sources and paleoceanographic implications, *Journal of Geophysical Research: Oceans*, *117*(C12), doi:10.1029/2012JC008161.

Romine, K., and G. Lombari (1985), Evolution of Pacific circulation in the Miocene: Radiolarian evidence from DSDP Site 289, *Geological Society of America Memoirs*, *163*, 273-290, doi:10.1130/MEM163-p273.

Saunders, A. D., J. G. Fitton, A. C. Kerr, M. J. Norry, and R. W. Kent (2013), The North Atlantic Igneous Province, in Large Igneous Provinces: Continental, Oceanic, and Planetary Flood Volcanism, edited, 45-93, *American Geophysical Union*, doi:10.1029/GM100p0045.

Scher, H. D., and E. E. Martin (2006), Timing and Climatic Consequences of the Opening of Drake Passage, *Science*, *312*(5772), 428-430, doi:10.1126/science.1120044.

Schmitz, W. J. (1996), *On the world ocean circulation. Volume II, The Pacific and Indian Oceans/a global update*, Woods Hole, Mass. : Woods Hole Oceanographic Institution.

Scudder, R. P., R. W. Murray, J. C. Schindlbeck, S. Kutterolf, F. Hauff, M. B. Underwood, S. Gwizd, R. Lauzon, and C. C. McKinley (2016), Geochemical approaches to the quantification of dispersed volcanic ash in marine sediment, *Progress in Earth and Planetary Science*, *3*(1), 1, doi:10.1186/s40645-015-0077-y.

Shevenell, A. E., J. P. Kennett, and D. W. Lea (2008), Middle Miocene ice sheet dynamics, deep-sea temperatures, and carbon cycling: A Southern Ocean perspective, *Geochemistry, Geophysics, Geosystems*, *9*(2), doi:10.1029/2007GC001736.

Sloan, L. C., D. K. Rea, S. C. Calif Univ, and U. Michigan (1996), Atmospheric Carbon Dioxide and Early Eocene Climate: A General Circulation Modeling Sensitivity Study, *Palaeogeography, Palaeoclimatology, Palaeoecology*, *119*(199623), 275-292.

Sluijs, A., et al. (2008), Eustatic variations during the Paleocene-Eocene greenhouse world, *Paleoceanography*, *23*(4), PA4216, doi:10.1029/2008PA001615.

Sluijs, A., et al. (2006), Subtropical Arctic Ocean temperatures during the Palaeocene/Eocene thermal maximum, *Nature*, *441*(7093), 610-613, doi:http://www.nature.com/nature/journal/v441/n7093/suppinfo/nature04668_S1.html.

Staudigel, H., P. Doyle, and A. Zindler (1985), Sr and Nd isotope systematics in fish teeth, *Earth and Planetary Science Letters*, *76*(1–2), 45-56, doi:http://dx.doi.org/10.1016/0012-821X(85)90147-5.

Stichel, T., M. Frank, J. Rickli, and B. A. Haley (2012), The hafnium and neodymium isotope composition of seawater in the Atlantic sector of the Southern Ocean, *Earth and Planetary Science Letters*, *317*, 282-294.

Tachikawa, K., C. Jeandel, and M. Roy-Barman (1999), A new approach to the Nd residence time in the ocean: the role of atmospheric inputs, *Earth and Planetary Science Letters*, *170*(4), 433-446, doi:http://dx.doi.org/10.1016/S0012-821X(99)00127-2.

Talley, L. (1993), Distribution and Formation of North Pacific Intermediate Water, *Journal of Physical Oceanography*, *23*(3), 517-537, doi:10.1175/1520-0485(1993)023<0517:DAFONP>2.0.CO;2.

Talley, L. (2003), Shallow, Intermediate, and Deep Overturning Components of the Global Heat Budget, *Journal of Physical Oceanography*, *33*(3), 530-560, doi:10.1175/1520-0485(2003)033<0530:SIADOC>2.0.CO;2.

Talley, L. (2013), Closure of the Global Overturning Circulation Through the Indian, Pacific, and Southern Oceans: Schematics and Transports, *Oceanography*, *26*(1), 80-97, doi:10.5670/oceanog.2013.07.

Taylor, S. R., and S. M. McLennan (1985), The continental crust : its composition and evolution : an examination of the geochemical record preserved in sedimentary rocks, Oxford; Boston: Blackwell Scientific; Palo Alto, California: Fistributors, USA and Canada, Blackwell Scientific, 1985.

Thomas, D. J. (2004), Evidence for deep-water production in the North Pacific Ocean during the early Cenozoic warm interval, *Letters of Nature*, *430*.

Thomas, D. J. (2005), Reconstructing ancient deep-sea circulation patterns using the Nd isotopic compostion of fossil fish debris, *Geological Society of America, Special Paper 305*.

Thomas, D. J., and R. K. Via (2007), Neogene evolution of Atlantic thermohaline circulation: Perspective from Walvis Ridge, southeastern Atlantic Ocean, *Paleoceanography, 22*(2), doi:10.1029/2006PA001297.

Thomas, D. J., M. Lyle, T. C. Moore, and D. K. Rea (2008), Paleogene deepwater mass composition of the tropical Pacific and implications for thermohaline circulation in a greenhouse world, *Geochemistry, Geophysics, Geosystems*, *9*(2), doi:10.1029/2007GC001748.

Thomas, D. J., R. Korty, M. Huber, J. A. Schubert, and B. Haines (2014), Nd isotopic structure of the Pacific Ocean 70–30 Ma and numerical evidence for vigorous ocean circulation and ocean heat transport in a greenhouse world, *Paleoceanography*, *29*(5), 2013PA002535, doi:10.1002/2013PA002535.

van de Flierdt, T., M. Frank, A. N. Halliday, J. R. Hein, B. Hattendorf, D. Günther, and P. W. Kubik (2004a), Deep and bottom water export from the Southern Ocean to the Pacific over the past 38 million years, *Paleoceanography*, *19*(1), doi:10.1029/2003PA000923.

van de Flierdt, T., M. Frank, D.-C. Lee, A. N. Halliday, B. C. Reynolds, and J. R. Hein (2004b), New constraints on the sources and behavior of neodymium and hafnium in seawater from Pacific Ocean ferromanganese crusts, *Geochimica et Cosmochimica Acta*, *68*(19), 3827-3843, doi:http://dx.doi.org/10.1016/j.gca.2004.03.009.

Via, R. K., D. J. Thomas, E. Exxonmobil, A. Texas, and U. M (2006), Evolution of Atlantic Thermohaline Circulation: Early Oligocene Onset of Deep-Water Production in The North Atlantic, *Geology*, *34*(6), 441-444.

Whittaker, J.M., Mulle, R.D., Leitchenkov, G., Stagg, H., Sdrolias, M., Gaina, C., and Goncharov, A., 2007, Major Australian–Antarctic plate reorganization at Hawaiian-Emperor Bend time, *Science*, 318, 83-86, doi:10.1126/science.1143769.

Woodruff, F., and S. M. Savin (1989), Miocene deepwater oceanography, *Paleoceanography*, *4*(1), 87-140, doi:10.1029/PA004i001p00087

Xie, R. C., F. Marcantonio, and M. W. Schmidt (2012), Deglacial variability of Antarctic Intermediate Water penetration into the North Atlantic from authigenic neodymium isotope ratios, *Paleoceanography*, *27*(3).

Zachos, J. C., G. R. Dickens, and R. E. Zeebe (2008), An early Cenozoic perspective on greenhouse warming and carbon-cycle dynamics, *Nature*, *451*(7176), 279-283.

Zachos, J. C., M. Pagani, L. Sloan, E. Thomas, and K. Billups (2001), Trends, Rhythms, and Aberrations in Global Climate 65 Ma to Present, edited, 686, American Society for the Advancement of Science.

Zika, J. D., F. Laliberté, L. R. Mudryk, W. P. Sijp, and A. J. G. Nurser (2015), Changes in ocean vertical heat transport with global warming, *Geophysical Research Letters*, *42*(12), 4940.